Exploring the dual role of *Mangifera indica* L. in regulating immune response and pain persistence in inflammatory bowel diseaseRunning title: Immunomodulatory and analgesic roles of *Mangifera indica* L. in IBD

Elena Lucarini, Anna Schettino, Noemi Marigliano, Clara Ciampi, Martina Smimmo, Francesca Romano, Antonio Paolillo, Luana Izzo, Jenefa Begum, Adel Abo Mansour, Nunzia Iaccarino, Antonio Randazzo, Karin Vicente Greco, Raffaele Scarpa, Francesco Caso, Asif Jilani Iqbal, Mariarosaria Bucci, Carla Ghelardini, Lorenzo Di Cesare Mannelli, Anella Saviano, Francesco Maione

PII: S1043-6618(25)00198-7

DOI: https://doi.org/10.1016/j.phrs.2025.107773

Reference: YPHRS107773

To appear in: *Pharmacological Research*

Received date: 19 March 2025
Revised date: 7 May 2025
Accepted date: 8 May 2025

Please cite this article as: Elena Lucarini, Anna Schettino, Noemi Marigliano, Clara Ciampi, Martina Smimmo, Francesca Romano, Antonio Paolillo, Luana Izzo, Jenefa Begum, Adel Abo Mansour, Nunzia Iaccarino, Antonio Randazzo, Karin Vicente Greco, Raffaele Scarpa, Francesco Caso, Asif Jilani Iqbal, Mariarosaria Bucci, Carla Ghelardini, Lorenzo Di Cesare Mannelli, Anella Saviano and Francesco Maione, Exploring the dual role of *Mangifera indica* L. in regulating immune response and pain persistence in inflammatory bowel diseaseRunning title: Immunomodulatory and analgesic roles of *Mangifera indica* L. in IBD, *Pharmacological Research,* (2025) doi:https://doi.org/10.1016/j.phrs.2025.107773

Research paper

Exploring the dual role of *Mangifera indica* L. in regulating immune response and pain persistence in inflammatory bowel disease

Elena Lucarini[a,†], Anna Schettino[b,†], Noemi Marigliano[b], Clara Ciampi[a], Martina Smimmo[c], Francesca Romano[c], Antonio Paolillo[c], Luana Izzo[c], Jenefa Begum[d], Adel Abo Mansour[e], Nunzia Iaccarino[c], Antonio Randazzo[c], Karin Vicente Greco[f,g], Raffaele Scarpa[h], Francesco Caso[h], Asif Jilani Iqbal[d], Mariarosaria Bucci[c], Carla Ghelardini[a], Lorenzo Di Cesare Mannelli[a], Anella Saviano[b,‡,*] and Francesco Maione[b,i,‡,*].

[a]*Department of Neuroscience, Psychology, Drug Research and Child Health - NEUROFARBA - Section of Pharmacology and Toxicology, University of Florence, Viale Pieraccini 6, 50139, Florence, Italy.*
[b]*ImmunoPharmaLab, Department of Pharmacy, School of Medicine and Surgery, University of Naples Federico II, Via Domenico Montesano 49, 80131, Naples, Italy.*
[c]*Department of Pharmacy, University of Naples Federico II, School of Medicine and Surgery, Via Domenico Montesano 49, 80131, Naples, Italy.*
[d]*Department of Cardiovascular Sciences, College of Medicine and Health, University of Birmingham, Birmingham, B15 2TT, UK.*
[e]*Department of Clinical Laboratory Sciences, College of Applied Medical Sciences, King Khalid University, Abha 62521, Saudi Arabia.*
[f]*University College London (UCL), Division of Surgery and Interventional Science, Royal Free Hospital Campus, UK*.
[g]*Department of Engineering of Materials and of Bioprocesses, School of Chemical Engineering, University of Campinas (UNICAMP), Av. Albert Einstein 500, CEP 13083-852 Campinas, SP, Brazil.*
[h]*Rheumatology Unit, Department of Clinical Medicine and Surgery, University of Naples Federico II, Via Domenico Montesano 49, 80131, Naples, Italy.*
[i]*Nutraceuticals and Functional Foods Task Force, Department of Pharmacy, School of Medicine and Surgery, University of Naples Federico II, Via Domenico Montesano 49, 80131, Naples, Italy.*

[†]These authors share first authorship.

[‡]These authors share senior authorship.

*****Corresponding authors: **Anella Saviano**, Assistant Professor of *ImmunoPharmaLab*, Department of Pharmacy, School of Medicine and Surgery, University of Naples Federico II, Via Domenico Montesano 49, 80131, Naples, Italy. Phone: (+39) 081678429. E-mail: anella.saviano@unina.it. **Francesco Maione**, Head of *ImmunoPharmaLab* & Nutraceuticals and Functional Foods Task Force, Department of Pharmacy, School of Medicine and Surgery, University of Naples Federico II, Via Domenico Montesano 49, 80131, Naples, Italy. Phone: (+39) 081678429. E-mail: francesco.maione@unina.it.

Abstract

Inflammatory bowel disease (IBD), encompassing ulcerative colitis and Crohn's disease, is characterized by chronic intestinal inflammation and immune dysregulation, driven mainly by Th1 and Th17 cells and sustained by pro-inflammatory cyto-chemokines. This inflammatory milieu is associated with visceral pain, a key symptom affecting patient quality of life. Addressing both gut inflammation/immunity and visceral pain is crucial for improving IBD therapy. This study assessed the therapeutic potential of *Mangifera indica* L. extract (MIE), a mangiferin-rich formulation, in a DNBS-induced colitis model in rats. MIE treatment administered either simultaneously or post-DNBS induction, significantly reduced pathogenic Th1 and Th17 cell infiltration, along with pro-inflammatory cytokines (IL-1β, TNF-α) and chemokines (CXCL1, CXCL2), though histopathology showed no significant improvements in tissue healing . Additionally, MIE restored microbiota-derived short-chain fatty acids (acetate and butyrate) in colon and faecal samples. Importantly, MIE alleviated post-inflammatory visceral hypersensitivity, reducing the abdominal withdrawal reflex (AWR) to colorectal distension (CRD), after either acute or repeated treatment. These findings suggest that MIE, in the context of nutraceuticals and functional foods, shows promise as a dual-action therapeutic strategy for complementary and/or adjuvant therapy in IBD.

Keywords: Functional foods, inflammatory bowel disease, mangiferin, *Mangifera indica* L., nutraceuticals, visceral hypersensitivity.

Declaration of competing interest. This article has been conducted and written in the absence of any commercial or financial relationships that could be construed as a potential conflict of interest.

Running title: Immunomodulatory and analgesic roles of *Mangifera indica* L. in IBD

Abbreviations: AIF, all-ion fragmentation; AWR, abdominal withdrawal reflex; BSA, bovine serum albumin; C5a, complement component 5a; CD, Crohn's disease; CE, collision energy; cLP, colonic lamina propria; CNS, central nervous system; CRD, colorectal distension; CXCL1, CXC motif chemokine ligand 1; CXCL2, CXC motif chemokine ligand 2; DAMPs, damage-associated molecular patterns; DMSO, dimethyl sulfoxide; DNBS, 2,4-dinitrobenzenesulfonic acid; DW, dry weight; EDTA, ethylenediaminetetraacetic acid; EGCs, enteric glial cells; EGTA, ethylene glycol-bis (β-aminoethyl ether)-N,N,N', N' tetra acetic acid; EI-MS, electron ionization mass spectrometry; ESI, electrospray ionization; FA, formic acid; FBS, foetal bovine serum; GAE, gallic acid equivalents; GC-MS, gas chromatography-mass spectrometry; G-CSF, granulocyte colony stimulating factor; GFAP, glial fibrillary acidic protein; HBSS, Hanks' balanced salt solution; HMDB, Human Metabolome Database; ^{1}H-NMR, proton nuclear magnetic resonance; HSP, heat shock protein; IBD, inflammatory bowel disease; IBS, irritable bowel syndrome; IFN-γ, interferon-gamma; IL, interleukin; i.r., intrarectally; LIX, lipopolysaccharide-induced CXC chemokine; LPM, Lvpimang; MCP-5, monocyte chemoattractant protein-5; MCPs, monocyte chemoattractant proteins; MCs, mast cells; M-CSF, macrophage colony-stimulating factor; MIE, *Mangifera indica* L. extract; MIG, monokine induced by interferon-gamma; MIP-2, macrophage inflammatory protein-2; MSI, metabolomics standards initiative; PBS, phosphate-buffered saline; PCA, principal component analysis; PFTBA, perfluorotributylamine; PMSF, phenylmethylsulfonyl fluoride; p.o., orally; RANTES, regulated on activation, normal T cell expressed and secreted; RI, retention index; RT, room temperature; SCFAs, short-chain fatty acids; SDF-1, stromal derived growth factor-1; Th, T helper; TIMP-1, tissue inhibitor of metalloproteinases-1; TLRs, toll-like receptors; TMSCN, trimethylsilyl cyanide; TNF-α, tumor necrosis factor alpha; TPC, total phenolic content; Treg, regulatory T cells; TREM-1, triggering receptor expressed on myeloid cells; Tris-HCL, tris(hydroxymethyl)aminomethane hydrochloride; UC, ulcerative colitis; UHPLC Q-Orbitrap HRMS,ultra-high-performance liquid chromatography-Q-Orbitrap high-resolution mass spectrometry**.**

Main Text

1. Introduction

Immunological colitis refers to chronic inflammation of the colon caused by a dysregulation of the immune system. It is commonly associated with inflammatory bowel disease (IBD), including ulcerative colitis (UC) and Crohn's disease (CD). These disorders are characterized by an inappropriate immune response to gut microbiota and intestinal epithelial cells, leading to chronic relapsing intermittently inflammation and tissue damage. Symptoms such as abdominal pain, diarrhoea, weight loss, and fatigue significantly affect patients'

quality of life, often leading to psychological distress, including anxiety and depression [1]. Noteworthy, in one third of IBD patients, abdominal pain persists beyond flare-ups and optimal treatment of the intestinal disease. Moreover, due to its complex and multifactorial nature, post-inflammatory pain is refractory to classic pain-relieving drugs, hence the need for new therapeutic approaches [2].

Although the precise aetiology of immunological colitis is multifactorial, the interaction between genetic predisposition, environmental factors, and immune system dysfunction plays a critical role in the disease initiation and progression [3].

Recent studies have deepened our understanding of the mechanisms underlying inflammation in immunological colitis. Key immune cells, including T lymphocytes, macrophages, and dendritic cells contribute to the inflammatory cascade by secreting pro-inflammatory cytokines, including tumor necrosis factor-alpha (TNF-α), interleukin (IL)-1, and IL-17 [4]. These cytokines recruit additional immune cells to the site of inflammation, perpetuating the cycle of immune activation and tissue destruction [5]. The chronic inflammatory environment also activates nociceptors (pain receptors) in the gut wall, contributing to abdominal pain, a key characteristic of colitis [6]. Pain in immunological colitis is not merely a result of tissue damage, but is also influenced by visceral hypersensitivity, a heightened sensitivity of the gut to normal physiological stimuli, such as distention or peristalsis [7]. This condition is thought to result from alterations in the gut-brain axis, which involves bidirectional communication between the gastrointestinal tract and the central nervous system (CNS) [8]. Neuroplastic changes in both gut and brain have been shown to enhance pain perception in patients with IBD [9]. It is now well established that chronic inflammation in the gut leads to both peripheral and central pain sensitization, contributing to the severity and persistence of symptoms [10]. Moreover, psychological factors such as stress and anxiety can modulate pain perception, creating a vicious cycle where pain leads to more stress, which in turn worsens the clinical symptoms [10]. Understanding the interaction between these factors is critical for developing comprehensive treatment strategies.

Despite the clear link between inflammation and pain in immunological colitis, much remains to be understood about the specific molecular and cellular mechanisms driving these processes. While therapies targeting inflammation, such as TNF inhibitors and IL-12/IL-23 inhibitors, have been effective in controlling disease activity, their impact on pain management remains less clear [11]. Additionally, the role of gut microbiota in modulating both immune responses and pain sensitivity is an emerging area of interest. Recent preclinical and clinical studies suggest that alterations in the gut microbiome-host interaction may influence both the inflammatory process and pain experience associated with IBD [12]. Among the emerging nutraceuticals and functional foods, *Mangifera indica* L., commonly known as mango, has shown promising potential in the management of IBD due its anti-inflammatory and immunomodulatory activities [13]. Mango, particularly its polyphenolic compounds such as mangiferin, exhibits strong anti-inflammatory, antioxidant, and immunomodulatory properties. Studies have demonstrated that a specific mango extract can reduce the expression of pro-inflammatory cytokines, such as TNF-α, IL-1β, and IL-6, which are central to the inflammatory process in IBD [14]. Furthermore, *Mangifera indica* has been shown to improve gut barrier function and modulate the gut microbiota, thereby reducing intestinal inflammation and promoting gut health. These properties suggest that mango could be a valuable addition to the therapeutic arsenal for IBD, particularly as an adjunct to conventional therapies. The integration of nutraceuticals and functional foods, such as *Mangifera indica* L., into the treatment regimen for IBD holds promise, offering complementary approaches that can help to manage symptoms, reduce inflammation, and improve gut health with fewer side effects when compared to long-term pharmacological treatments.

As a final objective and proof-of-concept of this study, we characterized three endemic Italian cultivars of *Mangifera indica*, designated as Keitt, Kent, and Palmer, by analyzing their primary and secondary metabolite profiles. Emphasis was placed on polyphenol content and, specifically, on the quantification of mangiferin. This targeted evaluation provides a foundation for the chemical and pharmacological translatability of our findings, highlighting the importance of local cultivar monitoring for agro-food quality control. Such an approach could foster the development of standardized nutraceuticals and/or novel foods, promoting their commercialization while ensuring adherence to high-quality standards.

2. Materials and methods

2.1. Reagents and chemicals

Mangifera indica L. extract (MIE, 90% mangiferin, batch number: CMGD-C-A091434) was supplied and certified by L.C.M. Trading S.p.A. (Milan, Italy) (the technical datasheet specification is reported in

Supplementary Fig. 1)and chemically characterized (**Supplementary Fig. 2**) in our previous study [15]. Bovine serum albumin (BSA), dimethyl sulfoxide (DMSO), 2,4-dinitrobenzenesulfonic acid (DNBS), KH_2PO_4, K_2HPO_4, NaN_3 and TSP were purchased from Sigma-Aldrich Co. (now under Merck, Darmstadt, Germany). Isoflurane was purchased from VIRBAC S.r.l., Milan, Italy. Foetal bovine serum (FBS), phosphate-buffered saline (PBS) and RPMI-1640 cell medium were obtained from SIAL (Rome, Italy), while ACK Lysing Buffer from Gibco Invitrogen Compounds (Paisley, Scotland). For flow cytometry analysis, fixation and permeabilization buffer was purchased from ThermoFisher Scientific (Carlsbad, CA), while FACS buffer and conjugated antibodies were from BioLegend (London, UK). Unless otherwise stated, all the other reagents were from BioCell (Milan, Italy).

2.2. Animals

For all the experiments described below, male Sprague–Dawley rats (Envigo, Varese, Italy), weighing approximately 220–250 g at the beginning of the experimental procedure, were used. Animals were housed in CeSAL (Centro Stabulazione Animali da Laboratorio, University of Florence, Florence, Italy) and used at least 1 week after their arrival. Four rats were housed per cage (size 26 × 41 cm); animals were fed a standard laboratory diet and tap water *ad libitum*, and kept at 23 ˚C ± 1 ˚C with a 12 h light/dark cycle, light at 7 a.m. All animal manipulations were carried out according to the Directive 2010/63/EU of the European Parliament and the European Union Council (22 September 2010) on the protection of animals employed for scientific purposes. The ethical policy of the University of Florence complies with the Guide for the Care and Use of Laboratory Animals of the US National Institutes of Health (NIH Publication number 85–23, revised 1996, University of Florence assurance number: A5278-01). Formal approval to conduct the described experiments was obtained from the Animal Subjects Review Board of the University of Florence (Italy) and the Italian Ministry of Health (388/2021-PR). Experiments involving animals have been reported according to ARRIVE guidelines. Experimental study groups were randomized, and their assessments were carried out by researchers blinded to the treatment groups. All efforts were made to minimize animal suffering and to reduce the number of employed animals.

2.3. DNBS-induced colitis model and experimental design

Colitis was induced in rats in conformity with the method described by Lucarini *et al*. [16]. During a brief period of anaesthesia with isoflurane (2%), 30 mg of DNBS (Merck Life Science, Milan, Italy) dissolved in 0.25 ml of 50% ethanol was intrarectally (i.r.) injected using a polyethylene PE-60 catheter inserted 8 cm proximal to the anus. Vehicle + vehicle control rats received an intrarectal injection of saline solution (0.25 ml). The effect of acute administration of MIE [1, 10, 30, 100 mg kg^{-1} orally (p.o.)] or corresponding vehicle (DMSO/saline 1:3 w/w as the minimum concentration required to enable solubilization and to devoid any anti-inflammatory activity *per se* [17] on visceral pain was assessed on Day 14 and 21, by using different subgroup of animals, according to the experimental setting shown in **Fig. 1A**. The route of administration, as well as the selected dosage(s) of MIE, were determined based on current literature, including findings from our previous studies [13, 15]. Two different experimental protocols of administration were adopted to evaluate the effect of repeated MIE treatment on the development and persistence of visceral pain in DNBS-treated rats. MIE treatment started concomitantly to DNBS injection (Day 0) and continued for 7 days or started 7 days after DNBS and continued for 14 days, as described in the experimental scheme in **Fig. 2A** and **2C**, respectively. Visceral pain assessments were performed on Day 7, 14, and 21 post DNBS injection, 24 h after the last treatment with MIE or vehicle. Once visceral pain assessments were completed, animals were sacrificed to collect faeces, colon and spleen tissues and lumbar segments of spinal cord for further *ex vivo* analysis.

2.4. Assessment of visceral sensitivity by abdominal withdrawal response (AWR)

Visceral pain sensitivity to colorectal distension (CRD) was assessed via AWR measurement using a semi-quantitative score as previously described in conscious animals by Lucarini *et al*. [16]. Briefly, rats were anesthetized with isoflurane (2%) and a lubricated latex balloon (length: 4.5 cm), attached to polyethylene tubing, assembled to an embolectomy catheter and connected to a syringe filled with water were inserted through the anus into the rectum and descending colon of rats. The tubing was taped to the tail to hold the balloon in place. Then rats were allowed to recover from the anaesthesia for 15 min. AWR measurement consisted of visual observation of animal responses to graded CRD (0.5, 1, 2, and 3 ml) by a blinded observer who assigned the following scores: No behavioural response to CRD (0); Immobile during CRD and occasional head clinching at stimulus onset (1); Mild contraction of the abdominal muscles, but the absence of abdomen lifting from the platform (2); Observed strong contraction of the abdominal muscles and lifting of the abdomen off the platform (3); Arching of the body and lifting of the pelvic structures and scrotum (4).

2.5. Isolation of colonic lamina propria (cLP) cells and splenocytes

cLP cells were isolated from colonic specimens according to previously described protocols [13]. Briefly, colons were removed and flushed several times with ice-cold PBS to remove intestinal content opened longitudinally and cut into small segments. Tissues were then incubated three times with pre-warmed cell dissociation solution made with Hanks' balanced salt solution (HBSS), FBS 5%, ethylenediaminetetraacetic acid (EDTA) 2 mM, and HEPES 10 mM for 30 min at 37 ˚C. Subsequently, to obtain cLP cells, colonic pieces were minced and treated with a digestion cocktail containing 1.5 mg ml^{-1} collagenase type IV (c.n.: C5138, Sigma-Aldrich Co.) and 0.1 mg ml^{-1} DNase I (c.n.: LS006342, Worthington-Biochem, New Jersey, USA) in RPMI 1640/10% FBS for 45 min at 37 ˚C with continuous stirring [18-20]. cLP cells were then filtered through a cell strainer with a 70-µm nylon mesh (Biologix, Ohio, USA) and washed with RPMI 1640/10% FBS, whereas splenocytes were isolated from the spleens in PBS and passed through a 40 µm-mesh-sized cell strainer (Corning, Arizona, USA) to obtain single cells after lysing of red blood cells by ACK buffer [21, 22]. Collected cells (cLP and splenocytes) were washed in PBS for total cell count. Cell number was determined by TC20 automated cell counter (Bio-Rad, Milan, Italy) using Bio-Rad's disposable slides, TC20 trypan blue dye (0.4% trypan blue dye w/v in 0.81% sodium chloride and 0.06% PBS) and a CCD camera to count cells based on the analyses of capture images. Isolated cLP cells were then analysed by flow cytometry analysis.

2.6. Flow cytometry analysis

Cells collected from digested colon tissues were washed in FACS buffer (PBS containing 1% BSA and 0.02% NaN_2) and incubated with eBioscience™ Fixable Viability Dye eFluor 780 (Thermo Fisher Scientific; c.n.: 65-0865-14) before the staining with fluorescence-conjugated antibodies. Specifically, cLP cells were stained with the following antibodies (all from BioLegend, London, UK): anti-CD3 PE (1:200; clone 1F4), anti-CD4 APC (1:200; clone W3/25), anti-CD8 FITC (1:200; clone OX-8) and anti-CD25 FITC (1:200; clone OX-39) for 60 min at 4 ˚C. After washing, cells were fixated, permeabilized, and stained intracellularly with anti-IL-17A PE (1:200; clone eBio17B7, eBioscience™), anti-interferon-gamma (IFN-γ PE; 1:200; clone DB-1) and anti-FOXP3 PE (1:200: clone 150D, both from BioLegend) antibodies. T helper (Th)1, Th17 and regulatory T cells (Treg) populations were defined as $CD4^+IFN\text{-}\gamma^+$, $CD4^+IL\text{-}17^+$ and $CD4^+CD25^+FOXP3^+$ cells respectively, according to the flow cytometry procedure previously described [15]. Furthermore, for the characterization of neutrophils and monocytes, cLP cells were surface stained with the following conjugated antibodies: LY6B.2 (7/4) FITC (1:200; clone 7/4) and LY6G APC (1:200; clone 1A8). Neutrophils and monocytes were defined as LY6B.2 $(7/4)^+LY6G^{hi}$ and LY6B.2 $(7/4)^+LY6G^{lo}$ populations respectively. At least 1×10^4 cells were analysed per sample, dead cells were excluded using cell viability marker, and positive and negative populations were determined based on the staining obtained with related IgG isotypes. Flow cytometry was performed on BriCyte E6 flow cytometer (Mindray Bio-Medical Electronics, Nanshan, China) using MRFlow and FlowJo software operation [23]. Flow cytometry strategy for neutrophils, monocytes, Th1 and Th17 subsets is reported in **Supplementary Fig. 3A-D**.

2.7. Faecal metabolome analysis by proton nuclear magnetic resonance (^{1}H-NMR) spectroscopy

Faecal samples (30 mg), collected on Day 21, from all experimental conditions were re-suspended in milliQ water, at a faecal weight to the water volume of ratio 1:2 and extracted by mixing with phosphate buffer prepared as described below. Briefly, 1.5 M solutions of KH_2PO_4 and K_2HPO_4 were prepared in milliQ water and mixed using magnetic stirrers at room temperature (RT) until complete dissolution. The two solutions, KH_2PO_4 and K_2HPO_4 were mixed in a 1:4 (v/v) ratio. Then, TSP and NaN_3 were added to the phosphate buffer at concentrations of 1 mg ml^{-1} and 0.13 mg ml^{-1}, respectively. The obtained solution was mixed using magnetic stirrers at RT for 10 min and stored overnight to ensure pH equilibration. 100 ml of this buffer was mixed with 900 ml of milliQ water to obtain the buffer used in this analysis [24]. After centrifugation (14000 g, at 37 ˚C) for 30 min, the supernatants were collected for ^{1}H-NMR measurements. A total of 65 µl of D_2O was added to the faecal extracts, vortexed briefly and transferred into 5-mm NMR tubes. All ^{1}H-NMR spectra were acquired at 298 K on a Bruker Avance NEO 600 MHz spectrometer (Bruker Biospin Gmbh, Rheinstetten, Germany) equipped with a QCI cryo-probe set for 5 mm sample tubes and an autosampler (SampleJet). The ^{1}H NMR spectra of faecal extracts were acquired with Topspin 4.1 (Bruker Biospin GmbH, Rheinstetten, Germany), using the 'noesypr1d' pulse sequence allowing for a quantitative evaluation even close to the water signal, which was presaturated at 4.698 ppm. NMR samples were stabilized at 298 K for 300 s, inside the probe, before starting the experiment. An acquisition time of 2.62 s, a relaxation delay of 4 s, receiver gain of 101, 128 scans, 4 dummy scans and a spectral width of 12500 Hz (20.8287 ppm) were employed. All samples were automatically tuned, matched, and shimmed. Prior to Fourier transformation, the free induction decays were

multiplied by an exponential function equivalent to a 0.3-Hz line-broadening factor. Then, the transformed spectra were automatically corrected for phase and baseline distortions and calibrated using TopSpin built-in processing tools. The assignment of the metabolites was achieved by (i) analysis of literature data [24, 25]; (ii) comparison with the chemical shifts of the metabolites in the Human Metabolome Database (HMDB); (iii) peak fitting routine within the spectral database in Chenomx NMR Suite 8.4 software package (Chenomx, AB, Canada) in its evaluation version.

2.8. Colon metabolome analysis by gas-chromatography coupled with mass spectroscopy (GC-MS)

Colon tissues from all experimental conditions, collected on Day 21, were submitted to a dual phase extraction procedure as reported elsewhere [26, 27]. Briefly, a mixture of cold water and methanol was added to each sample. In particular, portions of colon (30 mg) were mixed with 100 µl of cold water and 320 µl of cold methanol. Then, a homogenising step was needed to break up the tissues and let the partition of the metabolites in the extracting solvents. An ULTRA-TURRAX® tissue homogeniser (IKA® T10 basic) was employed for this purpose. After this step, 320 µl of cold chloroform was added to the homogenized colon samples, which were first briefly vortexed and then centrifuged at 4000 g at 4 ˚C for 15 min. This procedure generated a two-phase extract: the aqueous upper phase containing hydrophilic metabolites, while apolar metabolites as lipid molecules moved in the organic lower phase. The upper and lower phases were separated and transferred into different tubes. Finally, solvents were completely removed from both fractions using a vacuum concentrator. Only the hydrophilic phase was considered in this study and submitted to gas chromatography-mass spectrometry (GC-MS) analysis. A total 60 µl of final metabolites extract from each sample was put in a glass insert, dried first in a SpeedVac Concentrator (Thermo Fisher Scientific Co., Waltham, MA), for 4 h, and then put in the lyophiliser, overnight. The glass inserts were sealed with airtight magnetic lids into GC-MS vials and derivatised by addition of 60 µl of trimethylsilyl cyanide (TMSCN). Derivatisation and injection were fully automated using a PAL autosampler with Robotic Tool Change system (CTC Analytics, Zwingen, Switzerland) integrated to the GC-MS-TOF (Pegasus BT, LECO Corporation, Saint Joseph, MI). The GC-MS consisted of an Agilent 7890B GC (Agilent Technologies, Santa Clara, CA) and a time-of-flight mass spectrometer (LECO Corporation, Saint Joseph, MI). After the addition of the derivatisation reagent, samples were transferred into the agitator of the AS and incubated at 40 ˚C for 40 min at 750 rpm. This procedure ensures precise derivatisation time and reproducible sample injections. Immediately after derivatisation, 1 ml of the derivatised sample was injected in splitless mode into the injection port. The septum purge flow and purge flow were set to 25- and 15-ml min^{-1}, respectively. The injection port temperature was set to 250 ˚C. GC separation was performed on a Rxi-5MS 5% Phenyl 95% Dimethylpolysiloxane column (30 m with I.D. 0.25 mm and film thickness 0.25 mm) (Restek, Bellefonte, PA). The initial temperature of the GC oven was set to 40 ˚C and held for 2 min, followed by heating at 12 ˚C min^{-1} until 320 ˚C and kept for 8 min, making the total run time 33.3 min [26]. Mass spectra were recorded in the range of 45–600 m/z with an acquisition rate of 10 spectra/s, and MS detector and ion source were switched off during the first 6.4 min of solvent delay time. The transfer line and ion source temperature were set to 280 and 250 ˚C, respectively. Helium (grade 6.0; SOL Group, Caserta, Italy) was used as carrier gas, at a constant flow rate of 1 ml min^{-1}. The mass spectrometer was tuned according to manufacturer's recommendation using perfluorotributylamine (PFTBA). The autosampler and GC-MS were controlled using vendor software PAL Sample Control (CTC Analytics, Zwingen, Switzerland) and ChromaTOF (LECO Corporation, Saint Joseph, MI), respectively. Two technical replicates were prepared for each sample (for a total of 18 samples); they were randomised prior to derivatisation and GC–MS analysis. In order to monitor the instrument performance, an alkane mixture standard sample (all even C10–C40 alkanes in hexane) was employed. The raw GC TOF-MS data was processed by the ChromaTOF® Sync software version 1.1.5.1 (LECO Corporation, Saint Joseph, MI) that deconvolutes mass spectra and performs peak identification using NIST11 library (NIST, Gaithersburg, MD). The library search was set to return top 10 hits with EI-MS (electron ionization mass spectrometry) match of >80% using normal-forward search and with a mass threshold of 20. Deconvoluted peaks were aligned across all samples considering a retention time shift allowance of 80% of all pooled control samples. In this way, final datasets consisting of 50 metabolites for colon samples were obtained. The identification computed by the ChromaTOF was classified according to the levels indicated by the metabolomics standards initiative (MSI), (i) level 1 if the peaks are confirmed using authentic standards, (ii) level 2 when the peaks are identified based on their EI-MS match ≥80 (%) and retention index (RI) match (±30), and (iii) level 3 when the peaks are identified based on their EI-MS match ≥65 (%). In our case, no authentic standards were employed and only metabolites identified at level 2 have been considered for further analysis.

2.9. Metabolomics data processing and analysis

Metabolomics data from faeces and colon were processed independently and then combined to recover correlations. In particular, ^{1}H-NMR spectra from faecal samples were imported into MATLAB (R2021a; Mathworks, Natick, Massachusetts, USA), and spectral regions above 10 ppm and below 0 ppm were removed because they contained only noise. To correct for spectral misalignment, an interval-based alignment step was carried out using the icoshift algorithm [28] and choosing the acetate singlet at 1.90 ppm as the reference signal. To reduce model complexity and enhance interprertability, the peak areas of well-resolved and confidently assigned resonances from 34 selected metabolites were manually integrated. This process generated a data matrix made of 9 rows (samples) x 34 columns (metabolites) as listed in**Supplementary Fig. 4**. The resulting data matrix was imported into the PLS toolbox version 8.6.1 (Eigenvector Research, Manson, Washington, USA) within the MATLAB environment, normalized using Norm1, autoscaled, and subjected to principal component analysis (PCA). Similarly, colon-derived samples acquired via GC-MS were organized into a data matrix of 9 rows and 50 columns (**Supplementary Fig. 5**), normalized using Norm1, autoscaled, and analyzed by PCA.
Subsequently, a low-level data fusion [29] approach was applied by concatenating the faecal and colon data matrices, resulting in a fused matrix containing 9 rows (samples) and 84 columns (metabolites from both colon and faecal samples).
This combined matrix was then analyzed by PCA following two pre-processing steps: group scaling and autoscaling. Group scaling (via the gscale function in MATLAB) ensured equal contribution of each data block to the final model, indipendent of the number of variables. Autoscaling (also known as “unit variance scaling”) ensured that all variables had an equal wight in the model. Finally, PCA was performed, and scores and loadings plots were generated.

2.10. Preparation of colonic tissue homogenates

Portions of colons (1 cm) from all experimental conditions, collected on Day 7 and Day 21, were homogenized in ice-cold tris(hydroxymethyl)aminomethane hydrochloride (Tris-HCL) buffer (20 mM, pH 7.4) containing 0.32-M sucrose, 1 mM EDTA, 1 mM ethylene glycol-bis (β-aminoethyl ether)-N,N,N’, N’ tetra acetic acid (EGTA), 1 mM phenylmethylsulphonyl fluoride (PMSF), 1 mM sodium orthovanadate, and one tablet of Complete™ Protease Inhibitor Cocktail (c.n.: 04 693 116 001, Roche) per 50 ml of buffer, sonicated on ice and centrifuged (4500 g, at 4 ˚C) for 10 min. Total proteins within the supernatants were quantified using a Bradford protein assay (Bio-Rad) [30]. Supernatants from all experimental conditions were assayed for cytokines and chemokines protein arrays, according to manufacturer’s directions.

2.11. Cytokines and chemokines protein array assays

For cytokines (c.n.: ARY006) and chemokines (c.n.: ARY020) protein arrays (both from R&D System), equal volumes (1.5 ml) of pulled colon tissues homogenates from all experimental conditions (on Day 7 and Day 21) were incubated with the pre-coated proteome profiler array membranes according to the manufacturer's instructions. Dot plots were visualized using an enhanced chemiluminescence detection kit and Image Quant 400 GE Healthcare software (GE Healthcare, Milan, Italy) and the resulting data were quantified using GS 800 imaging densitometer software (Biorad, Segrate, Italy) as previously described [15].

2.12. Histochemical and immunofluorescence analysis of colon

The evaluation of colon damage was performed as previously reported [31]. The colon length was measured after the explant of the tissue. For the histological analysis, the colon was fixed in 4% paraformaldehyde for 24 h, dehydrated in alcohol, included in paraffin, and cut into 5 µm sections. Microscopic evaluations of colon damage (mucosal architecture loss, cellular infiltrate, muscle thickening, crypt abscess, and goblet cell depletion) were carried out on sections stained with haematoxylin/eosin (Bio-Optica, Milan, Italy). The infiltration of mast cells (MCs) and eosinophils was investigated on colon sections stained with GIEMSA (Bio-Optica, Milan, Italy). Digitalized images were collected by a Leica DMRB light microscope equipped with a DFC480 digital camera (40-400× magnification; Leica Microsystems, Wetzlar, Germany). The quantitative analysis was carried out by two blind investigators with the software ImageJ. For each animal, the cellular density (cell number/respective arbitrary field) of 6 independent arbitrary optical fields (0.1 mm^2) collected from the submucosa of each animal was measured. The analysis was performed on 4 (Day 7) or 6 (Day 21) animals *per group*. For the immunofluorescence analysis (Day 21), the colon was cut into 20 µm slices and the immunolabelling was performed according to standard protocols [31]. Selected slices from each animal, were incubated overnight at 4 ˚C with the following combination of primary antibodies, diluted in T-PBS/5% BSA (Sigma-Aldrich, Milan, Italy):

1) rat anti-FoxP3 monoclonal antibody (FJK-16s), eFluor™ 570, eBioscience™(41-5773-82; Invitrogen-Thermo Fisher Scientific, Milan, Italy; 1:100) + rabbit anti-CD4 polyclonal antibody (PA5-87425; Invitrogen-Thermo Fisher Scientific, Milan, Italy; 1:100).
2) rabbit anti-panaxonal marker PGP9.5 (ab108986, Abcam, UK; 1:500) + rat anti-FoXP3 monoclonal antibody (FJK-16s), eFluor™ 570, eBioscience™ (41-5773-82, Invitrogen-Thermo Fisher Scientific, Milan, Italy; 1:100).
2) rabbit anti-panaxonal marker PGP9.5 (ab108986, Abcam, UK; 1:500) + chicken anti-glial fibrillary acidic protein polyclonal antibody (GFAP, PA1-10004; Invitrogen-Thermo Fisher Scientific, Milan, Italy; 1:500).
The day after, slices were incubated for 2 h with secondary antibodies (1:500) labelled with Alexa Fluor 488, 568 or 647 (Invitrogen-Thermo Fisher Scientific, Milan, Italy), and then with DAPI to stain the nuclei. The slices were finally mounted with Fluoromount-G™ Mounting Medium (Thermo Fisher Scientific, Milan, Italy). Digitalized images were collected at 400× (mucosa) total magnification using a motorized Leica microscope DM6 B equipped with a DFC9000 GT camera, supported by a THUNDER Workstation 3D DCV and by the software LAS X (Leica Biosystems, Milan, Italy). Since, during set-upping (**Supplementary Fig. 6C**) all FoxP3 positive cells were $CD4^+$, Treg cells were detected through FoxP3 labelling in the following analyses. Areas of interaction between Treg cells (FoxP3-positive cells) and nerve endings (PGP9.5-related immunolabeling) were investigated. All images report cell nuclei marked with DAPI (grey). The quantitative analysis of colon PGP9.5-related immunofluorescence intensity and the number of GFAP-positive cells was performed by collecting independent fields (400×; 6-10 for each animal) from mucosal layer, analysing selected ROI and normalizing the data to the area of mucosa analysed with the software FIJI (NIH, Bethesda, MD, USA). The analysis was performed on 4-6 animals *per group*.

2.13. Bioactive compounds extraction

The bioactive compounds from different varieties of mango (Keitt, Kent and Palmer) of peel and pulp were extracted as previously reported [32]. Briefly 0.5 g of lyophilised sample was extracted with 5 ml of the EtOH:H_2O mixture (80:20, v:v). The mixture was vortexed for 2 min and sonicated for 15 min. Subsequently, the solution was agitated for 30 min and subjected to centrifugation at 5000 g for 5 min. The entire supernatant was collected, and the pellet was submitted to a second extraction using the same protocol. Finally, the two supernatants were combined, filtered through 0.2 µm filters and appropriately diluted by MeOH containing 0.1% formic acid (FA) prior to analysis.

2.14. Ultra-high-performance liquid chromatography-Q-Orbitrap high-resolution mass spectrometry (UHPLC Q-Orbitrap HRMS analysis)

The quali-quantitative profile of bioactive compounds was performed using a UHPLC system (Dionex UltiMate 3000, Thermo Fisher Scientific, Waltham, MA, United States) equipped with a degassing system, an autosampler device and a quaternary UHPLC pump coupled with a high-resolution mass spectrometry (Q-Exactive). Chromatographic separation was carried out with a thermostated (T=25 ˚C) Kinetex F5 (particle size 17 µm, 100 × 2.1 mm) column (Phenomenex, Castel Maggiore, Italy). The mobile phases consisted of water (A) and methanol (B), both containing 0.1% FA. The injection volume and flow rate were set to 5 µl and 0.4 ml min^{-1}, respectively. The gradient elution program was as follows: 0-0.5 min, 0% B; 0.5-1.0 min, 70% B; 1.0-7.8 min, 100% B; 7.8-8.3 min, 0% B; 8.3-10 min, 0% B. The total run time was 10 min. Mass spectrometry was performed on a Q-Exactive Orbitrap system equipped with an electrospray ionization (ESI) source operating in negative ion mode. Full ion MS and all-ion fragmentation (AIF) scan events were set. In full MS scan mode, the following conditions were fixed: scan range of 80-1,200 m/z; resolution power of 70,000 full width at half maximum; microscan set to 1; automatic gain control target of 1×10^6; maximum injection time of 200 ms; sheath gas flow rate of 35; auxiliary gas flow rate of 10; spray voltage set at 2.8 kV; capillary temperature maintained at 275 ˚C; S-lens RF level set to 50; and auxiliary gas heater temperature at 350 ˚C. In the AIF scan mode, the resolving power was configured as follows: scan range 80-1,200 m/z, resolution power of 17,500 full width at half maximum; microscan set to 1; automatic gain control target of 1×10^5; maximum injection time of 200 ms; sheath gas flow rate of 35; auxiliary gas flow rate of 10; spray voltage set at 2.8 kV; capillary temperature set at 275 ˚C; S-lens RF level set to 50 and auxiliary gas heater temperature at 350 ˚C. Collision energy (CE) was set within a range of 15 to 45 eV to achieve a representative product ion spectrum. Detection was achieved considering the exact mass with a mass error <5 ppm. Data analysis was performed using Xcalibur software 3.1.66.19 (Xcalibur, Thermo Fisher Scientific, Waltham, MA, United States) [33].

2.15. Total phenolic content (TPC) assay

The Folin-Ciocalteu method was used for determining the TPC following the procedure reported by Castaldo *et al*. [34]. Briefly, 500 µl of deionized water and 125 µl of the Folin-Ciocalteu reagent 2 N were added to 125

µl of extract. The tube was mixed and incubated for 6 min in dark conditions. Then 1.25 ml of 7.5% of sodium carbonate solution and 1 ml of deionized water were added. The reaction mixture was maintained in dark conditions for 90 min. Finally, the absorbance at 760 nm was measured through a spectrophotometer system. Results were expressed as mg of gallic acid equivalents (GAE)/g of dry weight (DW) sample.

2.16. Statistical analysis

Statistical analysis complies with the international recommendations on experimental design and analysis in pharmacology and data sharing and presentation in preclinical pharmacology. Data are presented as mean ± S.D. Normality was tested prior to analysis with one or two-way ANOVA followed by Bonferroni's or Dunnett's for multiple comparisons, where P≤0.05 was deemed significant. GraphPad Prism 8.4.3 (San Diego, CA, USA) software was used for analysis. Behavioural and histological results were expressed as mean ± S.E.M. The analysis of variance (ANOVA) was performed by one-way ANOVA with Bonferroni's significant difference procedure used for post-hoc comparisons. P values of less than 0.05 were considered significant. Data were analyzed using the "Origin 9" software (OriginLab, Northampton, MA). For *in vivo* studies, animal weight was used for randomization and group allocation to reduce unwanted sources of variations by data normalization. *In vivo* study was carried out to generate groups of equal size (n=5-6 of independent values) using randomisation and blinded analysis [13].

3. Results

3.1. Efficacy of MIE in the management of visceral pain associated with DNBS-induced colitis in rats

To delve deeper into anti-hyperalgesic efficacy of MIE, we used an established model of colitis induced by intrarectal injection of DNBS in rats, which recapitulates IBD in terms of pathophysiology and response to drugs [16]. The acute pain-relieving effect of MIE was evaluated 14 days and 21 days after DNBS injection, in the post-inflammatory and in the remission phase of colitis, according to the experimental scheme reported in **Fig. 1A**. Visceral pain was measured in animals by assigning a score to their AWR (0–4) to CRD (0.5–3 ml). Both 14 and 21 days after colitis induction, abdominal response to CRD in DNBS-treated animals was significantly higher than in the control group receiving the vehicle (**Fig. 1B** and **1C**, respectively). On day 14, the acute administration of MIE (1-100 mg kg^{-1} p.o.) effectively alleviated visceral hypersensitivity in DNBS-treated rats in a dose-dependent manner. MIE at 10, 30, and 100 mg kg^{-1} substantially reduced the abdominal response of animals to CRD, though only the effect of the higher dose was significant for all the distending volumes applied to the colon. The effect of the lower dose of MIE (1 mg kg^{-1}) on visceral pain was not significant, though the AWR score in response to 0.5-1 ml was still lower than that of DNBS animals administered with the vehicle (**Fig. 1B**). On Day 21, the acute administration of MIE 30 mg kg^{-1} continued to effectively relieve visceral hypersensitivity in DNBS-treated rats, whereas vehicle injection had no effect (**Fig. 1C**). Taken together, these data guided our decision to test MIE at a dose of 10 mg kg^{-1}, in alignment with the dosing strategy adopted in our previous studies[13, 15]. .

In a second experimental setup, we evaluated the efficacy of repeated MIE treatment in preventing the development of visceral pain associated with DNBS-induced colitis in rats. For this purpose, MIE (10 mg kg^{-1}) was administered daily, starting from DNBS induction (Day 0) and continuing the treatment for 7 consecutive days (during the acute inflammatory phase of colitis induced by DNBS). Visceral sensitivity was assessed on Day 7, 24 h after the last MIE administration in rats (experimental scheme; **Fig. 2A**). No difference in the AWR to CRD was observed between the group DNBS + vehicle and the group DNBS + MIE, the treatment was therefore ineffective in preventing the pain associated with colitis (**Fig. 2B**).

In the third experimental setup, we investigated the efficacy of the repeated treatment with MIE in counteracting the persistence of visceral pain in the remission phase of colitis caused by DNBS injection in rats. MIE (10 mg kg^{-1}) was administered daily in these animals, starting from Day 7 after the DNBS injection and continuing the treatment for 14 consecutive days. Visceral sensitivity was assessed on Day 7 (before starting MIE treatment), 14, and 21 (24 h after the last MIE administration; experimental scheme; **Fig. 2C**). Before treatment initiation, no differences were observed between the DNBS-injected groups, both of which exhibited a significant increase in visceral sensitivity compared to vehicle-injected control (**Fig. 2D-i**). On Day 14 and 21 (after 7 and 14 days of treatment, respectively; **Fig. 2D-ii** and **2D-iii**), DNBS-treated animals administered with MIE showed a significant reduction in the AWR in response to CRD. Moreover, on Day 21, visceral sensitivity in the DNBS + MIE group matched that of the control group (vehicle + vehicle), indicating a complete reversal of pain. (**Fig. 2D-iii**).

The 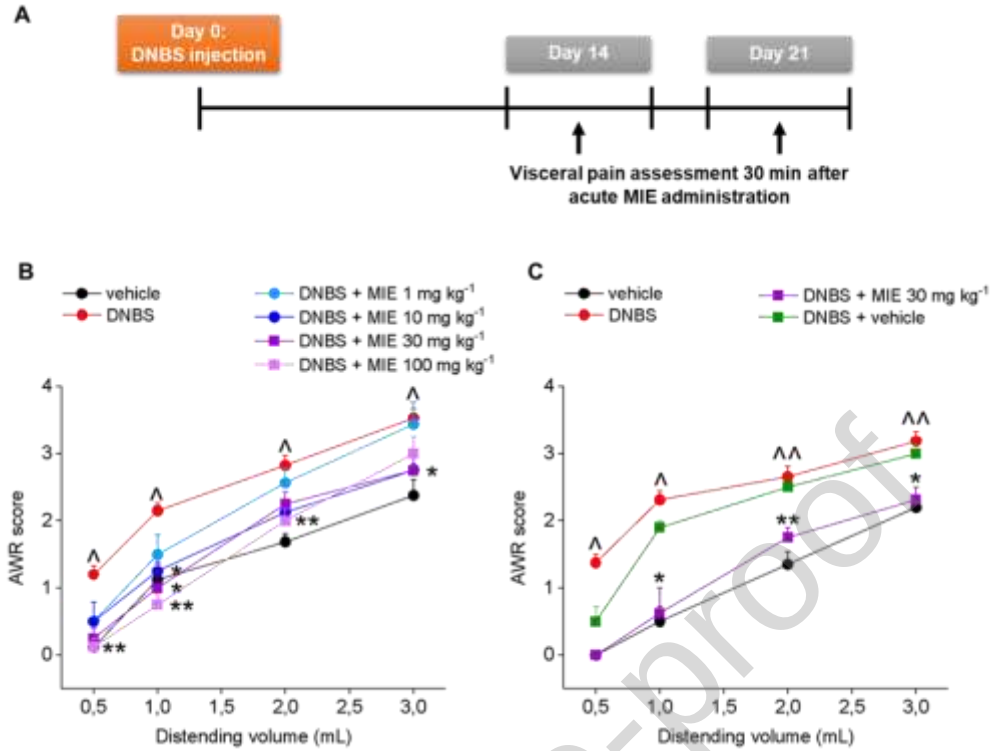

anti-hyperalgesic effect of repeated treatment with MIE emerged to be independent of tissue healing. Indeed, we observed shortening of colon length, together with the increase in microscopic damage scores and in mast cell density detected histologically, indicating that inflammatory damage to the colon of DNBS-treated animals [16], were not significantly modified by MIE treatment in either experimental paradigms (**Supplementary Fig. 7**).

Collectively, these results confirmed the therapeutic efficacy of MIE in the treatment of persistent visceral pain resulting from colon inflammation. It is important to note that the treatment was effective when administered in the post-inflammatory phase, but not in the acute phase of colitis. During the different phases (relapsing and remitting) of IBD [35] the immune response is altered. Since post-inflammatory or post-infection immune derangement have been reported to drive visceral pain persistence [36, 37], MIE anti-hyperalgesic effects may rely on mechanisms which target specific changes occurring in the immune response and neuroimmune interaction between the acute phase of inflammation and remission. This hypothesis prompted us to further investigate the immune responses in both experimental paradigms.

Fig. 1. Efficacy of MIE in alleviating persistent visceral pain resulting from DNBS-induced colitis in rats. Colitis was induced by the intrarectal injection of DNBS in rats. The effect of acute administration of MIE (p.o. 1-100 mg kg^{-1}) on visceral pain was assessed on Day 14 and 21 (**B** and **C**; post-inflammatory and remitting phases of colitis) according to the experimental setting shown in **A.** Visceral sensitivity was measured by scoring animals' abdominal withdrawal response (AWR) in response to colorectal distension (CRD) (0.5-3 ml), 30 min after MIE or vehicle administration. The values represent the mean ± S.E.M. of each group, n=4. The analysis of variance (ANOVA) was performed by one-way ANOVA with Bonferroni's significant difference procedure used for post-hoc comparisons. ^P≤0.05 and ^^P≤0.01 *vs* vehicle group. *P≤0.05 and **P≤0.01 *vs* DNBS group.

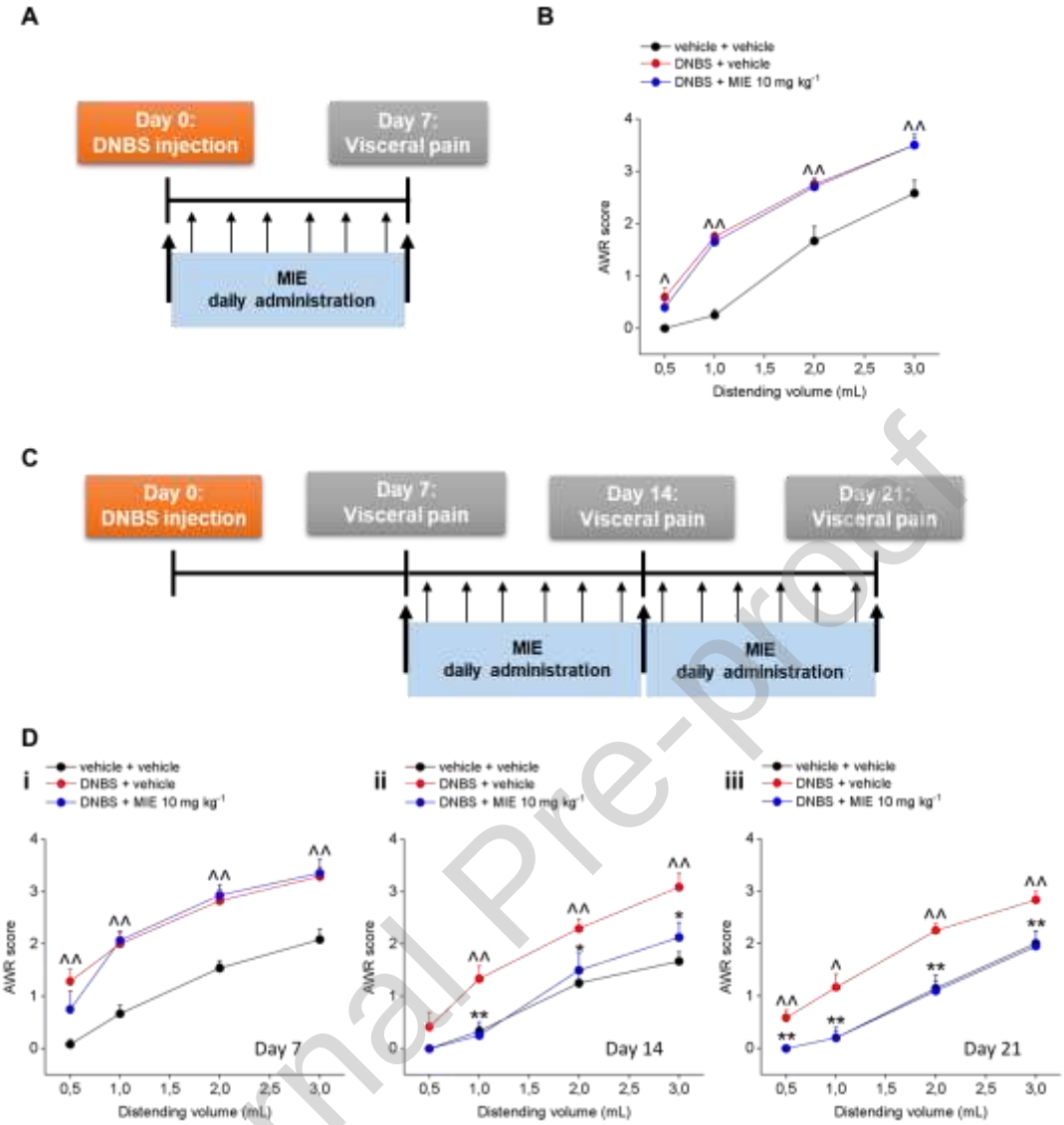

Fig. 2. Therapeutic potential of MIE in counteracting visceral pain persistence after colitis remission. Colitis was induced by the intrarectal injection of DNBS in rats. In the first experimental setting (**A**), animals were administered daily with MIE (p.o. 10 mg kg^{-1}) from Day 0 (induction of colitis) to Day 6, representing the acute phase of inflammation induced by DNBS. Visceral pain was assessed in rats on Day 7, 24 h after the last treatment (**B**). In the second experimental setting (**C**), MIE (p.o. 10 mg kg^{-1}) was administered starting from Day 7 to Day 20, representing the remission phase of colitis. Visceral pain was assessed in rats on Day 7 (before starting the treatment **D-i**), on Day 14 and 21 (**D-ii** and **D-iii;** 24 h after the last treatment). Visceral sensitivity was measured by scoring animals' abdominal withdrawal response (AWR) in response to colorectal distension (CRD) (0.5-3 ml). The values represent the mean ± S.E.M. of each group. First experimental setting: vehicle + vehicle, n=6; DNBS + vehicle, n=8; DNBS + MIE, n=5. Second experimental setting: vehicle + vehicle, n=6; DNBS + vehicle, n=6; DNBS + MIE n=6. The analysis of variance (ANOVA) was performed by one-way ANOVA with Bonferroni's significant difference procedure used for post-hoc comparisons. ^P≤0.05 and ^^P≤0.01 *vs* vehicle + vehicle group. *P≤0.05 and **P≤0.01 *vs* DNBS + vehicle group.

.3.2. MIE selectively modulates neutrophil and monocyte infiltration during the onset and progression of DNBS-induced colitis

Neutrophils and inflammatory monocytes are critical players in the early stages of inflammation, driving the initiation [38] and amplification of immune responses, particularly in conditions like IBD [39]. Tissue damage or disruption of epithelial barriers triggers the release of damage-associated molecular patterns (DAMPs) and

pro-inflammatory cytokines, such as IL-1β and TNF-α. These molecules recruit neutrophils to the site of injury via chemokine gradients, such as CXC motif chemokine ligand 1 (CXCL1) and CXC motif chemokine ligand 2 (CXCL2) [38, 40, 41]. While this response is essential for pathogen clearance, excessive neutrophil activation can lead to further tissue damage, worsening mucosal injury and promoting continued inflammation. This cascade is further amplified by the recruitment of inflammatory monocytes through monocyte chemoattractant proteins (MCPs), such as CCL2 [42].

This inflammatory environment is characterized by the continuous secretion of cytokines including TNF-α, IL-6, and IL-1β, which not only sustain neutrophil activity, but also perpetuate the inflammatory cycle through a feedback loop. Importantly, this environment fosters antigen presentation and facilitates crosstalk between the innate and adaptive immune systems. In the context of colitis, this translates to the infiltration of $CD4^+$ Th1 and $CD4^+$ Th17 cells, which contribute to the sustained immune response and tissue damage [43]. This complex interplay between immune cells underscores the role of neutrophils and inflammatory monocytes in driving the chronic inflammation seen in IBD.

Given the pivotal role of neutrophils and monocytes in driving inflammation, we characterized these innate immune subsets in cLP cells during DNBS-induced colitis in both the acute (7 days post-DNBS injection) and resolution (21 days post-DNBS injection) phases, as outlined in the experimental plan shown in **Fig. 3A** (**i** and **ii**, respectively). A significant increase in both total cells of cLP (**Fig. 3B-i**) and spleen (**Fig. 3B-ii**) were detected in DNBS-injected animals on Day 7 time point (**Fig. 3C** and **3D**). A similar profile was observed on Day 21, albeit with a lower absolute cell count in both compartments (**Fig. 3E** and **3F**). MIE treatment significantly decreased total cLP cells during the resolution phase (21 days post-DNBS injection), with a trend toward reduction observed in the early phase of inflammation. Systemically, MIE markedly reduced the number of splenocytes on Day 7, with a less pronounced reduction observed on Day 21 (**Fig. 3C-F**), confirming the immunomodulatory effects of MIE were mirrored systemically, as previously reported [13, 15]. Subsequently, considering the colon as the primary site of inflammation and the observed modulation in total infiltrated cells, we performed a detailed phenotypic characterization of innate immune populations using flow cytometry analysis at both time points. Specifically, total cells were gated, followed by single cells and live cells (refer to flow cytometry strategy in **Supplementary Fig. 3A** and **3C**) to identify neutrophil (LY6B.2 $(7/4)^+$/$LY6G^{hi}$) and monocyte (LY6B.2 $(7/4)^+$/$LY6G^{lo}$) subsets on Day 7 (**Fig. 3G-I**) and Day 21 (**Fig. 3J-L**).

We found that DNBS injection produced an intense infiltration of neutrophils and monocytes on Day 7 (**Fig. 3G-I**). During the resolution phase, both neutrophils and monocytes remained significantly higher compared to the vehicle group, but their total numbers had dramatically decreased (**Fig. 3J-L**). Specifically, neutrophil numbers were reduced by approximately 95%, while monocyte levels decreased by around 70%. These results are consistent with the role of neutrophils and monocytes as key players during the acute phase of inflammation, with their numbers decreasing as the immune response shifts towards resolution, allowing adaptive immunity to take over. MIE treatment significantly reduced the neutrophil population on Day 7 (**Fig. 3G** and **3H**), with a continued but non-significant trend by Day 21 (**Fig. 3J** and **3K**). Interestingly, a significant decrease in the monocytes population was observed only on Day 21 (**Fig. 3J** and **3L**), parallel to the MIE effect on visceral hyperalgesia. Collectively, these data suggest that MIE exerts a differential immunomodulatory effect on innate immune cell populations, with a stronger impact on neutrophils during the acute phase and on monocytes during the resolution phase, highlighting its potential to modulate distinct phases of the inflammatory response.

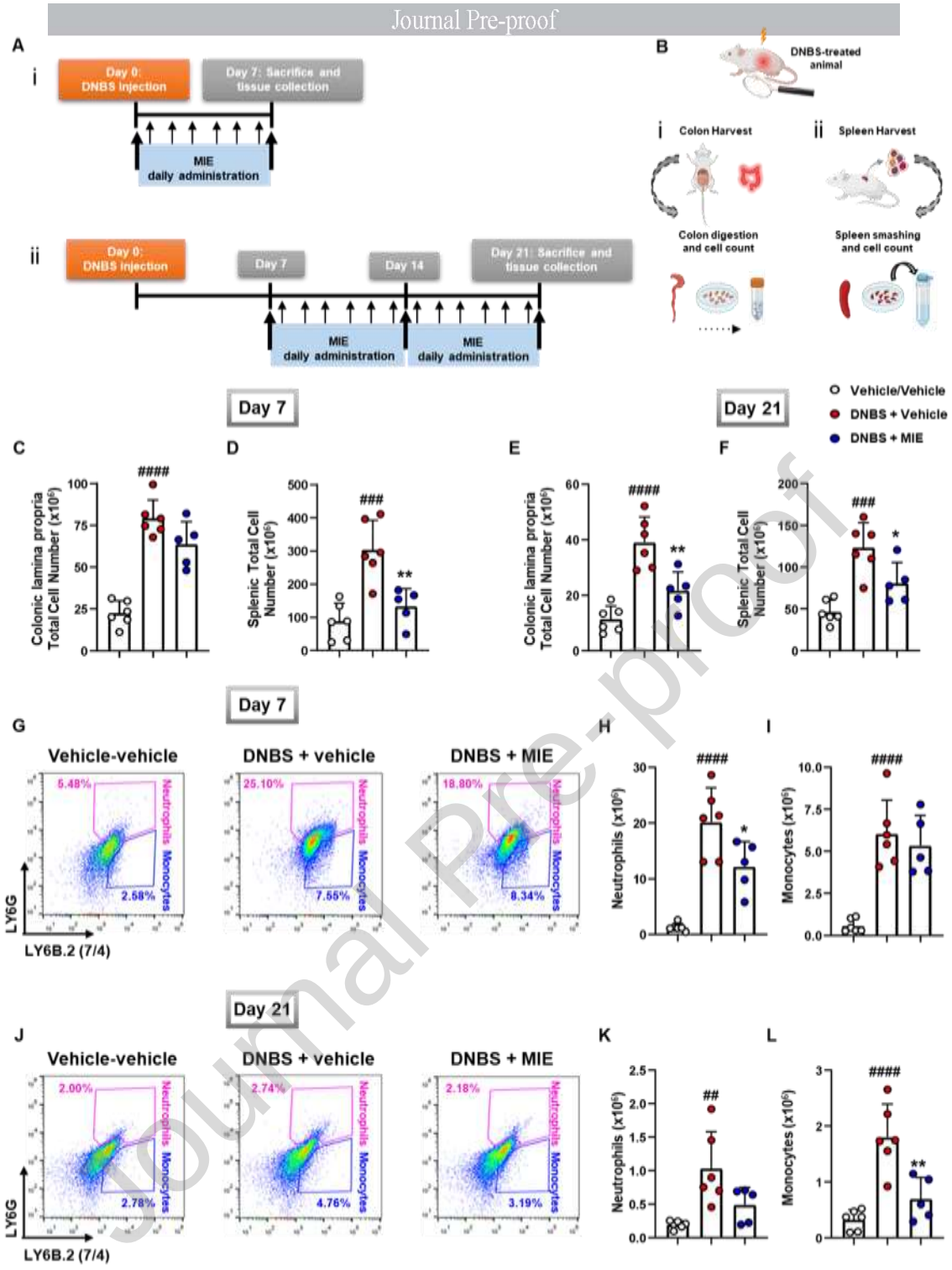

Fig. 3. Therapeutic potential of MIE in alleviating DNBS-induced colitis. Animals were injected with DNBS to induce colitis and administered daily with MIE (p.o. 10 mg kg^{-1}) according to two experimental settings shown in **A**: i) from Day 0 (induction of colitis) to Day 6, representing the acute phase of inflammation, and ii) from Day 7 (post-model induction) to Day 20, representing the resolution phase. Visceral sensitivity and viscero-motor response were assessed at indicated time points (**A**). Colon samples were harvested and enzymatically digested (**B-i**), while spleens were smashed to obtain single-cell suspensions (**B-ii**). Total cell count was performed for both cLP and spleen-derived cells on Day 7 (**C** and **D**) and Day 21 (**E** and **F**). Subsequently, flow cytometry analysis was employed to determine neutrophil and monocyte subsets in the cLP. For this purpose, cells were gated in their totality and singlet, and stained with Fixable viability dye (flow cytometry strategy reported in **Supplementary Fig. 3A** and **3C**) before the identification of neutrophil (LY6B.2 $(7/4)^{+}LY6G^{hi}$) and monocyte (LY6B.2 $(7/4)^{+}LY6G^{lo}$) populations on Day 7 (**G**) and Day 21 (**J**). FACS pictures are presented as dot plot (pseudocolor), whereas % of positive cells are reported on the respective gates (purple for neutrophils and blue for monocytes). Histograms indicate the total positive populations (expressed

as x10^6 and calculated from means of % of positive cells), in the different experimental conditions (Day 7: **H** and **I**; Day 21: **K** and **L**). Data are presented as means ± S.D. of n=5-6 rats per experimental group. Statistical analysis was conducted using one-way ANOVA followed by Bonferroni's for multiple comparisons. $^{\#\#}$P≤0.01, $^{\#\#\#}$P≤0.001, $^{\#\#\#\#}$P≤0.0001 *vs* vehicle + vehicle group; *P≤0.05, **P≤0.01 *vs* DNBS + vehicle group.

3.3. MIE modulates pathogenic Th1 and Th17 infiltration in the colonic lamina propria

Immune subsets of $CD4^+$T-cells, such as Th1 and Th17, play a crucial role in the pathogenesis of IBD, where their infiltration into intestinal tissue serves as a common hallmark of the disease. These T-cells, with the ability to develop memory against previously encountered antigens, along with the altered microbiota and a dysregulated innate immune response, are key drivers of the chronic relapsing-remitting nature of IBD [43]. To investigate the immunomodulatory activity of MIE, we evaluated its impact on Th1 and Th17 cell populations from digested colon tissues using flow cytometry analysis. Total cells were gated, followed by single cells and live cells (see flow cytometry strategy in **Supplementary Fig. 3B** and **3D**) to identify Th1 ($CD4^+$/IFN-γ^+) and Th17 ($CD4^+$/IL-17^+) subsets on Day 7 (**Fig. 4A-D**) and Day 21 (**Fig. 4E-H**).

Notably, colitis induced a significant increase in both Th1 and Th17 in cLP population on Day 7 (**Fig. 4A-D**), with comparable levels of infiltration observed for both subsets. By Day 21, the Th1 profile remained significantly elevated, while Th17 cells exhibited a significant reduction (**Fig. 4E-H**). Treatment with MIE significantly reduced both Th1 and Th17 populations at both time points. Specifically, a marked decrease was observed on Day 7 compared to untreated colitis (**Fig. 4A-D**), and this reduction persisted by Day 21, effectively attenuating the inflammatory response (**Fig. 4E-H**). The modulation of Th1/Th17 balance was reflected by significant differences in the total $CD4^+$ and cytotoxic $CD8^+$ cells at the early phase of inflammation, with MIE notably reducing both subsets (**Supplementary Fig. 8A-G**). On Day 21, MIE treatment continued to reduce $CD3^+$ and $CD4^+$ cells (**Supplementary Fig. 9A-G**), contributing to the observed modulation of immune cell dynamics.

Our data demonstrated that DNBS-induced colitis serves as a Th1-mediated inflammatory model, as evidenced by the predominance of Th1 cells in the later stages of disease progression, where they continue to play a central role in sustaining chronic inflammation [44]. In contrast, the marked decline in Th17 cells may reflect regulatory mechanisms designed to limit tissue damage or a shift in immune responses as the disease progresses. This variability could be attributed, in part, to temporally regulated cytokine responses [43], with early lesions exhibiting a predominantly Th1/Th17-like signature, while later stages tend to favour a more Th1-dominant response. Notably, the ability of MIE to downregulate both Th1 and Th17 populations underscores its potential as a promising nutraceutical approach, exerting a robust immunomodulatory effect that could help restore immune balance in the context of colitis.

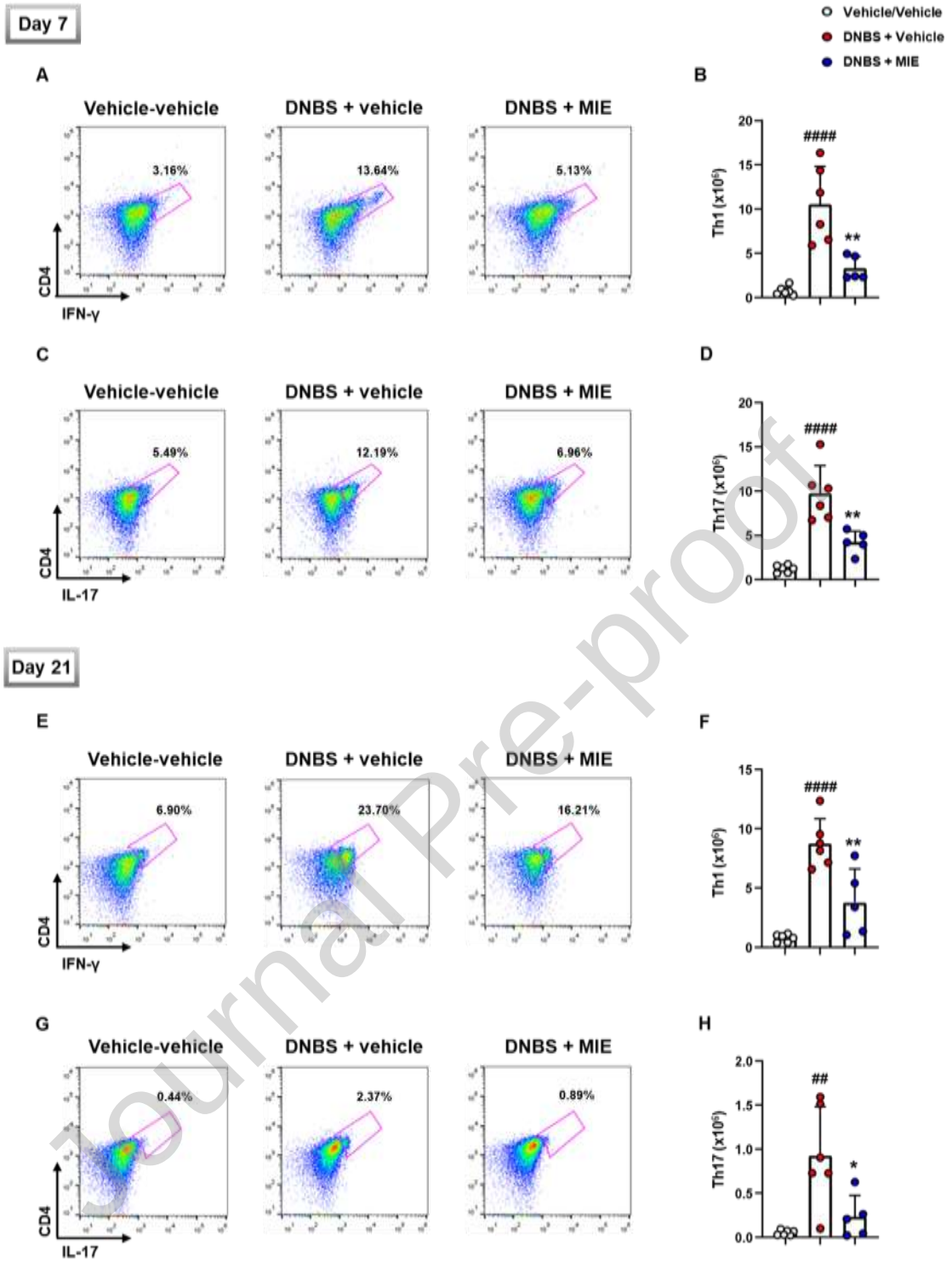

Fig.4. MIE modulation of Th1/Th17 cell dynamics in the colonic lamina propria. At the experimental end points (Day 7 and Day 21), isolated cLP cells from vehicle + vehicle, DNBS + vehicle and DNBS + MIE groups were analysed by flow cytometry analysis to determine Th1 and Th17 lymphocyte subsets. For this purpose, cells were gated in their totality and singlet, and stained with Fixable viability dye (flow cytometry strategy reported in **Supplementary Fig. 3B** and **3D**) before the identification of $CD4^+IFN\text{-}\gamma^+$ (**A** and **E**, Th1 population) and $CD4^+IL\text{-}17^+$ (**C** and **G**, Th17 population). FACS pictures are presented as dot plot (pseudocolor), whereas % of positive cells are reported on the respective gates. Histograms indicate the total positive populations (expressed as $x10^6$ and calculated from means of % of positive cells), in the different experimental conditions (Day 7: **B** and **D**; Day 21: **F** and **H**). Data are presented as means ± S.D. of n= 5-6 rats per experimental group. Statistical analysis was conducted using one-way ANOVA followed by Bonferroni's for multiple comparisons. $^{\#\#}P\leq0.01$, $^{\#\#\#\#}P\leq0.0001$ *vs* vehicle + vehicle group; $^*P\leq0.05$, $^{**}P\leq0.01$ *vs* DNBS + vehicle group.

3.4. MIE dampens the release of cyto-chemokines in colon tissue

Given the pivotal role of pro-inflammatory mediators in the pathogenesis of IBD [45-47], and to investigate their temporal dynamics, we next employed an ELISA Spot assay on colon tissues from Day 7 and Day 21 to assess if MIE influences the expression of cytokines and chemokines during the onset and progression of colitis. As shown in **Fig. 5**, colon homogenates from the DNBS group revealed a marked increase in pro-inflammatory cytokines (**Fig. 5A-D**) and chemokines (**Fig. 5E-H**) compared to the vehicle group, with distinct differences between Day 7 and Day 21.

On Day 7 (**Fig. 5A** and **5B**), there was a pronounced elevation in both cytokines and chemokines associated with acute inflammation and immune cell recruitment. Specifically, CC chemokines including JE (CCL2), MIP-1α (CCL3), and regulated on activation, normal T cell expressed and secreted (RANTES; CCL5) were significantly upregulated, indicating active recruitment of monocytes and inflammatory cells to the site of inflammation. Similarly, CXC chemokines, including KC (CXCL1), monokine induced by interferon-gamma (MIG; CXCL9), macrophage inflammatory protein-2 (MIP-2; CXCL2), and stromal derived growth factor-1 (SDF-1; CXCL12), exhibited substantial increases, reflecting a strong neutrophilic response. Additionally, pro-inflammatory cytokines IL-1β, TNF-α, IL-17, IL-23, IFN-γ, and immune activators complement component 5a (C5a), granulocyte colony stimulating factor (G-CSF), macrophage colony-stimulating factor (M-CSF), triggering receptor expressed on myeloid cells (TREM)-1 and IL-1ra were highly elevated, underscoring the activation of both innate immune responses and $CD4^+$ T-cell subsets, particularly Th1 and Th17 cells. These mediators are known to sensitize peripheral nociceptors, which can contribute to the visceral pain observed during the acute inflammatory phase of colitis. Despite the strong pro-inflammatory response, regulatory mediators such as IL-4, IL-13, IL-16, and tissue inhibitor of metalloproteinases-1 (TIMP-1) were modestly upregulated, suggesting an early, yet insufficient, attempt to counterbalance the inflammatory response. By Day 21 (**Fig. 5C** and **5D**), the cytokine profile shifted, showing a reduction in the intensity of inflammation. While pro-inflammatory mediators remained significantly elevated compared to the vehicle group, their levels were far lower than those on Day 7, indicating a decline in monocyte and neutrophil recruitment. However, certain mediators, including SDF-1, C5a, M-CSF, TREM-1, IL-16 and IL-1ra remained high. These factors may contribute to continued nociceptor sensitization and the persistence of Th1 cells, as previously observed in the phenotypical characterization [48]. Moreover, the exclusive expression of IL-2 on Day 21 (**Fig. 5C** and **5D**) could suggest an expansion of Tregs, which rely on IL-2 for their survival and function in suppressing chronic inflammation and restoring immune tolerance [49]. However, IL-2 can also sustain Th1 cell persistence, highlighting its dual role in balancing immune regulation and pro-inflammatory responses [50].

For chemokines, 6Ckine (CCL21), Eotaxin (CCL11), monocyte chemoattractant protein-5 (MCP-5; CCL12), lipopolysaccharide-induced CXC chemokine (LIX; CXCL5), and Chemerin were also highly expressed on Day 21 (**Fig. 5G** and **5H**), indicating the continued involvement of innate immunity in the inflammatory process, a finding that is further supported by the previous flow cytometry analysis. Finally, the significant upregulation of heat shock protein (HSP)60 on Day 21 (**Fig. 5G** and **5H**) reflects its dual role in chronic inflammation and immune regulation. As a DAMP, HSP60 can activate nociceptors through toll-like receptors (TLRs) on sensory neurons, thereby contributing to visceral pain [51]. Simultaneously, HSP60 supports the expansion and function of Tregs, promoting immune tolerance and potentially limiting further tissue damage [52]. This dual role underscores the complex interplay between immune responses and pain modulation in colitis. Importantly, treatment with MIE significantly modulated the expression of these cytokines and chemokines at both Day 7 and Day 21 (**Fig. 5A-H**), suggesting its potential to influence both the acute and chronic phases of inflammation, providing further evidence of its immunomodulatory properties. The complete panel of all cytokines and chemokines for Day 7 and 21 is shown in **Supplementary Fig. 10A-H**.

Our investigation into the temporal dynamics of pro-inflammatory mediators in DNBS-induced colitis revealed distinct cyto-chemokine expression profiles at acute (Day 7) and chronic (Day 21) phases. The initial phase was characterized by a pronounced elevation of pro-inflammatory cytokines and chemokines, indicating active immune cell recruitment and inflammation. By Day 21, although there was a general decline in these mediators, certain factors remained elevated, suggesting ongoing immune activity and potential nociceptor sensitization. Notably, treatment with MIE significantly modulated the expression of these pro-inflammatory mediators at both time points, underscoring its potential as an immunomodulatory agent in both acute and chronic phases of colitis.

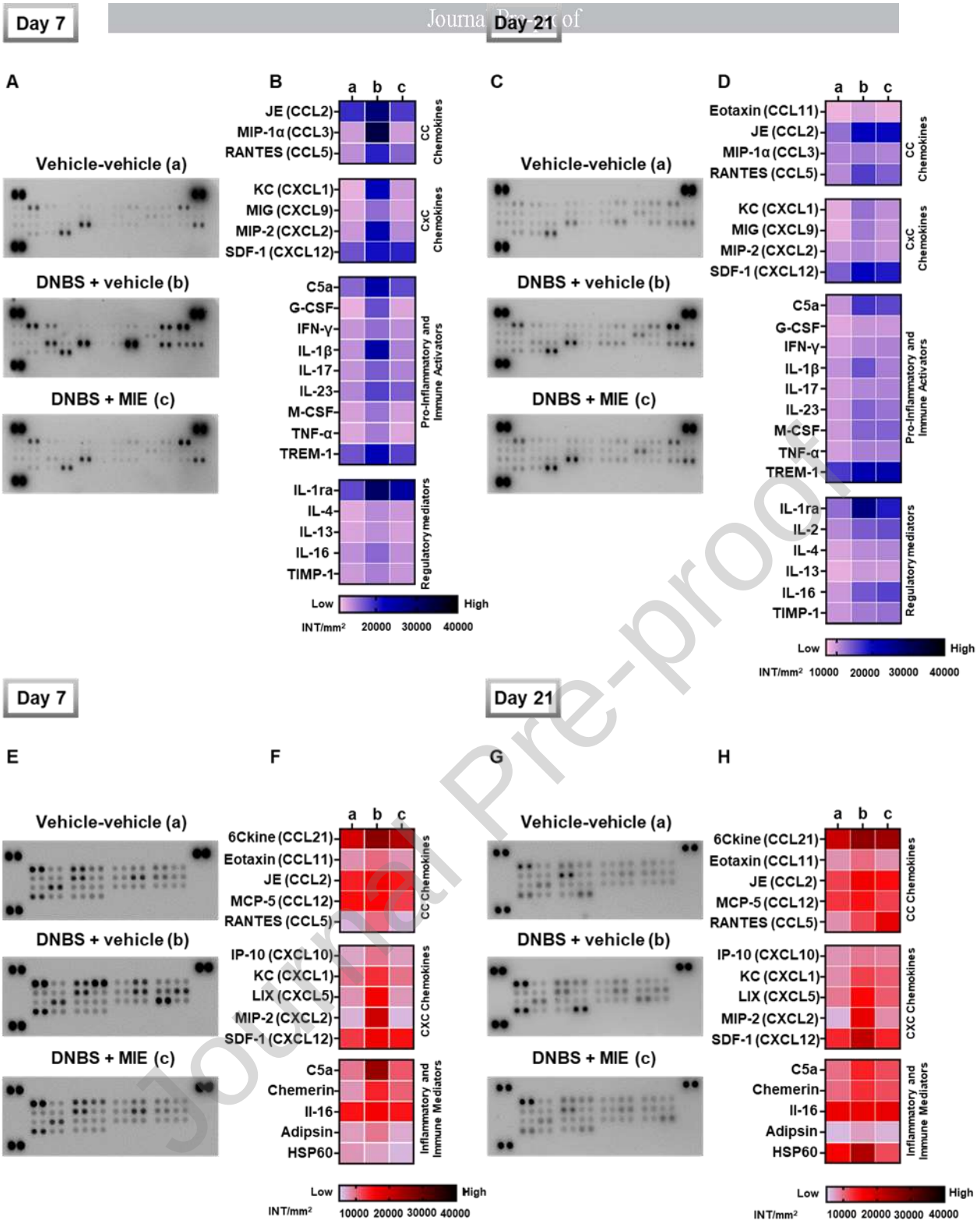

Fig. 5. MIE modification of colonic cyto-chemokines release. Supernatants of colon tissue homogenates from vehicle + vehicle (a), DNBS + vehicle (b) and DNBS + MIE (c) groups at the experimental end points (Day 7 and Day 21) were assayed using proteome profiler array kits, for the detection of cytokines (**A-D**) and chemokines (**E-H**). Densitometric analyses of cytokines (**B** and **D**) and chemokines (**F** and **H**) are presented as heatmaps with values expressed as INT/mm^2 (**B**, **F** and **D**, **H** respectively for Day 7 and Day 21). Data are presented as median ± S.D. (colormap: double gradient) of n=5-6 animals in each group pooled. Statistical analyses for Elisa Spot assays (detailed below) were performed by using two-way ANOVA followed by Dunnett's for multiple comparisons. *Cytokines Day 7*. P≤0.05 *vs* vehicle + vehicle group: IL-13. P≤0.01 *vs* vehicle + vehicle group: IL-4 and TIMP-1. P≤0.001 *vs* vehicle + vehicle group: IL-16. P≤0.0001 *vs* vehicle + vehicle group: JE, MIP1-α, RANTES, KC, MIG, MIP-2, SDF-1, C5a, GCS-F, IFN-γ, IL-1β, IL-17, IL-23, M-CSF, TNF-α, TREM-1 and IL-1ra. P≤0.05 *vs* DNBS + vehicle group: IL-13 and TIMP-1. P≤0.01 *vs* DNBS + vehicle group: MIG. P≤0.001 *vs* DNBS + vehicle group: IL-16. P≤0.0001 *vs* DNBS + vehicle group: JE, MIP1-α, RANTES, KC, MIP-2, C5a, GCS-F, IFN-γ, IL-1β, IL-17, IL-23, M-CSF, TNF-α, TREM-1 and IL-1ra. *Cytokines*

Day 21. P≤0.05 *vs* vehicle + vehicle group: Eotaxin, G-CSF, IFN-γ and IL-17. P≤0.01 *vs* vehicle + vehicle group: IL-4, IL-13, TIMP-1 and TNF-α. P≤0.001 *vs* vehicle + vehicle group: MIP-2. P≤0.0001 *vs* vehicle + vehicle group: JE, RANTES, KC, MIG, SDF-1, C5a, IL-1β, IL-23, M-CSF, TREM-1, IL-1ra, IL-2 and IL-16. P≤0.05 *vs* DNBS + vehicle group: IL-16, C5a and IL-23. P≤0.01 *vs* DNBS + vehicle group: MIP-2. P≤0.001 *vs* DNBS + vehicle group: RANTES and SDF-1. P≤0.0001 *vs* DNBS + vehicle group: KC, MIG, IL-1β and IL-1ra. *Chemokines Day 7*. P≤0.05 *vs* vehicle + vehicle group: JE, MCP-5, KC and SDF-1. P≤0.01 *vs* vehicle + vehicle group: RANTES. P≤0.001 *vs* vehicle + vehicle group: LIX. P≤0.0001 *vs* vehicle + vehicle group: 6Ckine, MIP-2, C5a, Chemerin, IL-16 and Adipsin. P≤0.05 *vs* DNBS + vehicle group: JE, MCP-5 and KC. P≤0.01 *vs* DNBS + vehicle group: 6Ckine and RANTES. P≤0.0001 *vs* DNBS + vehicle group: LIX, MIP-2, C5a, Chemerin, IL-16 and Adipsin. *Chemokines Day 21.* P≤0.05 *vs* DNBS + vehicle group: Eotaxin and MCP-5. P≤0.01 *vs* DNBS + vehicle group: KC, C5a and Chemerin. P≤0.001 *vs* DNBS + vehicle group: RANTES. P≤0.0001 *vs* DNBS + vehicle group: 6Ckine, JE, LIX, MIP-2, SDF-1 and HSP60. P≤0.05 *vs* DNBS + vehicle group: 6Ckine, Eotaxin, JE and C5a. P≤0.01 *vs* DNBS + vehicle group: MCP-5. P≤0.001 *vs* DNBS + vehicle group: LIX. P≤0.0001 *vs* DNBS + vehicle group: RANTES, MIP-2, SDF-1 and HSP60.

3.5. Effect of repeated treatment with MIE on neuroimmune interaction occurring within the mucosa of post-colitis rats

Building on the upregulation of key mediators of immune tolerance, we examined the phenotypic profile of Treg cells on Day 7 and Day 21 to explore their role in chronic inflammation and pain modulation in colitis, considering their crucial function in maintaining immune homeostasis [53-56]. Total cells were gated, followed by single cells and live cells (refer to flow cytometry strategy in **Supplementary Fig. 6A** and **6B**) to identify Treg ($CD4^+/CD25^+/FOXP3^+$) subset on Day 7 (**Fig. 6A** and **6B**) and Day 21 (**Fig. 6C** and **6D**) in cLP cells. We observed a significant reduction in Treg cells on Day 7 in rats with colitis (**Fig. 6A** and **6B**), indicating an early impairment of regulatory mechanisms in the acute phase of inflammation. This decline may be due to the highly pro-inflammatory environment, which could impair Treg survival or expansion. By Day 21, however, there was a notable increase in the absolute number of Treg cells (**Fig. 6C** and **6D**), suggesting a compensatory response aimed at restoring immune tolerance and controlling chronic inflammation. This late-phase expansion of Tregs may be driven in part by the persistence of inflammatory stimuli that support their survival and function including IL-2 and HSP60. Notably, MIE did not modulate Treg cell numbers on either Day 7 or Day 21 (**Fig. 6A-D**). To determine whether MIE influenced Treg functionality rather than their abundance, we further investigated its effects on the interaction between Treg cells and mucosal nerve endings.

Immunofluorescence analysis highlighted different areas of interaction between FoxP3-positive Treg cells, and nerve endings at the level of colonic mucosa in DNBS-treated animals remitting from colitis (Day 21). These areas of interaction were also present in MIE treated group, but they appeared to be sparser (**Fig. 6E**). Although further research is needed to prove this hypothesis, immune cells functionality and neuroimmune interaction might represent other potential targets of MIE.

Moreover, MIE treatment was able to significantly reduce the number of GFAP-positive enteric glial cells (EGCs) surrounding enteric nerves and infiltrating the mucosa of DNBS-treated animals (**Fig. 7A-D**). Enteric glia plays a key role in the crosswalk between sensory neurons and immune cells [57]. Several studies propose the involvement of enteric glia in the regulation of visceral sensitivity [58]. Notably, MIE treatment did not significantly alter Treg cell numbers at either time points. However, immunofluorescence analysis revealed that Treg cells are proximal to nerve endings within the colonic mucosa. At the same level, a decreased number of GFAP-positive EGCs was detected as a result of MIE treatment [59]. These findings suggest that MIE may modulate neuroimmune interactions and glial activity, contributing to its anti-inflammatory and analgesic effects in colitis.

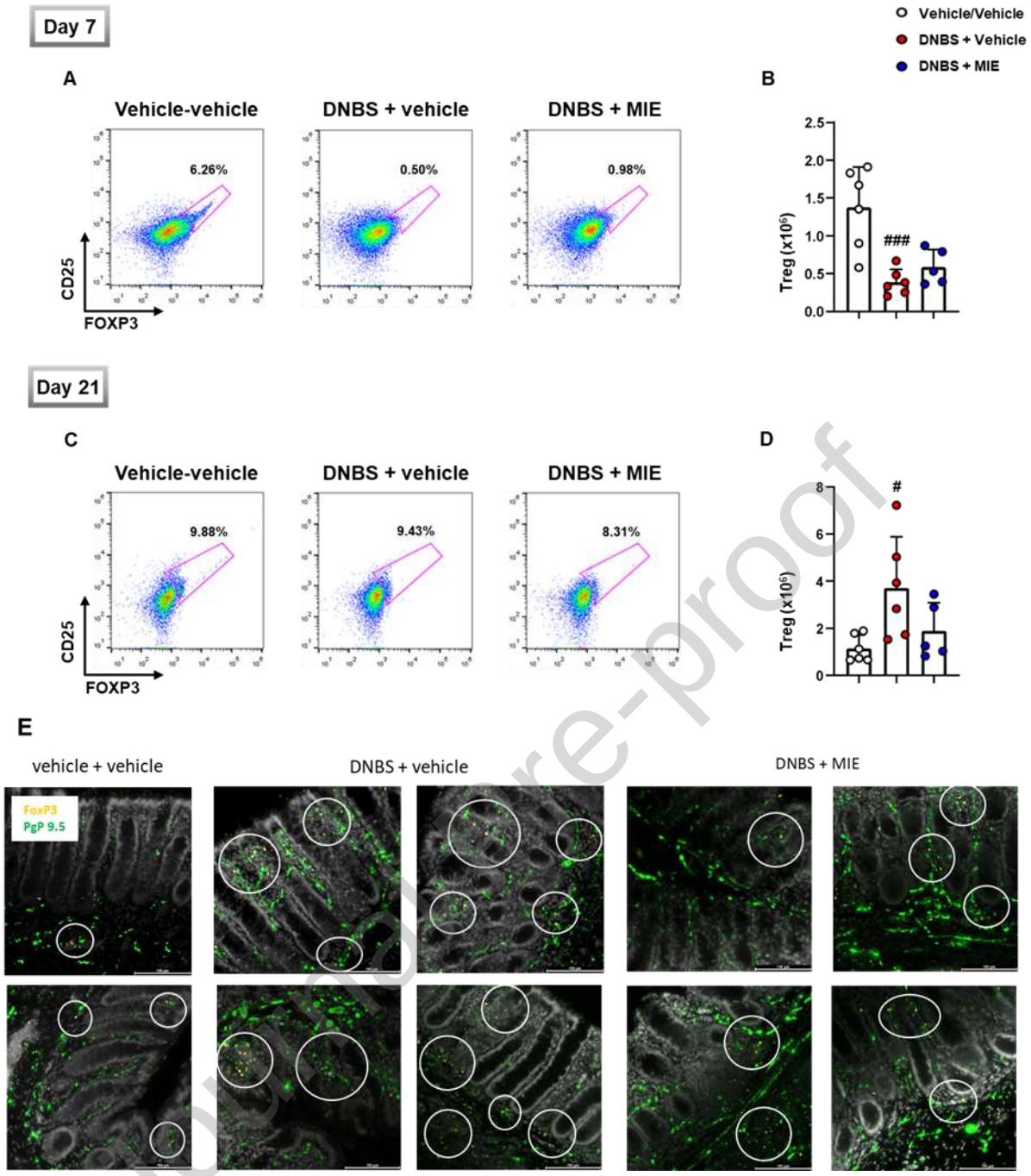

Revised Fig. 6. Modification of Treg dynamics within the mucosa of post-colitis rats and effect of MIE on the interaction between Treg cells and nerve endings. At the experimental end points (Day 7 and Day 21), isolated cLP cells from vehicle + vehicle, DNBS + vehicle and DNBS + MIE groups were analysed by flow cytometry analysis to determine Treg lymphocyte subsets. For this purpose, cells were gated in their totality and singlet and stained with Fixable viability dye (flow cytometry strategy reported in **Supplementary Fig. 6A** and **6B**) before the identification of $CD4^{+}CD25^{+}FOXP3^{+}$ cells (**A** and **C**, Treg population). FACS pictures are presented as dot plot (pseudocolor), whereas % of positive cells are reported on the respective gates. Histograms indicate the total positive populations (expressed as $x10^{6}$ and calculated from means of % of positive cells), in the different experimental conditions (Day 7: **B**; Day 21: **D**). Data are presented as means ± S.D. of n= 5-6 rats per experimental group. Statistical analysis was conducted using one-way ANOVA followed by Bonferroni's for multiple comparisons. $^{\#}P\leq0.05$, $^{\#\#\#}P\leq0.001$ *vs* vehicle + vehicle group. On Day 21, the distribution of positive cells for FoxP3 (Treg cells; marked yellow), and PGP 9.5 (nerve endings) within the mucosa was assessed by immunofluorescence analysis on colon sections (**E**). Areas of interaction between Treg cells and nerve endings were indicated by circling in the representative images. All images report cell nuclei marked with DAPI (grey). Four to six images (40x magnification) from the mucosa of each animal were examined (vehicle + vehicle, n=5; DNBS + vehicle, n=4; DNBS + MIE, n=6).

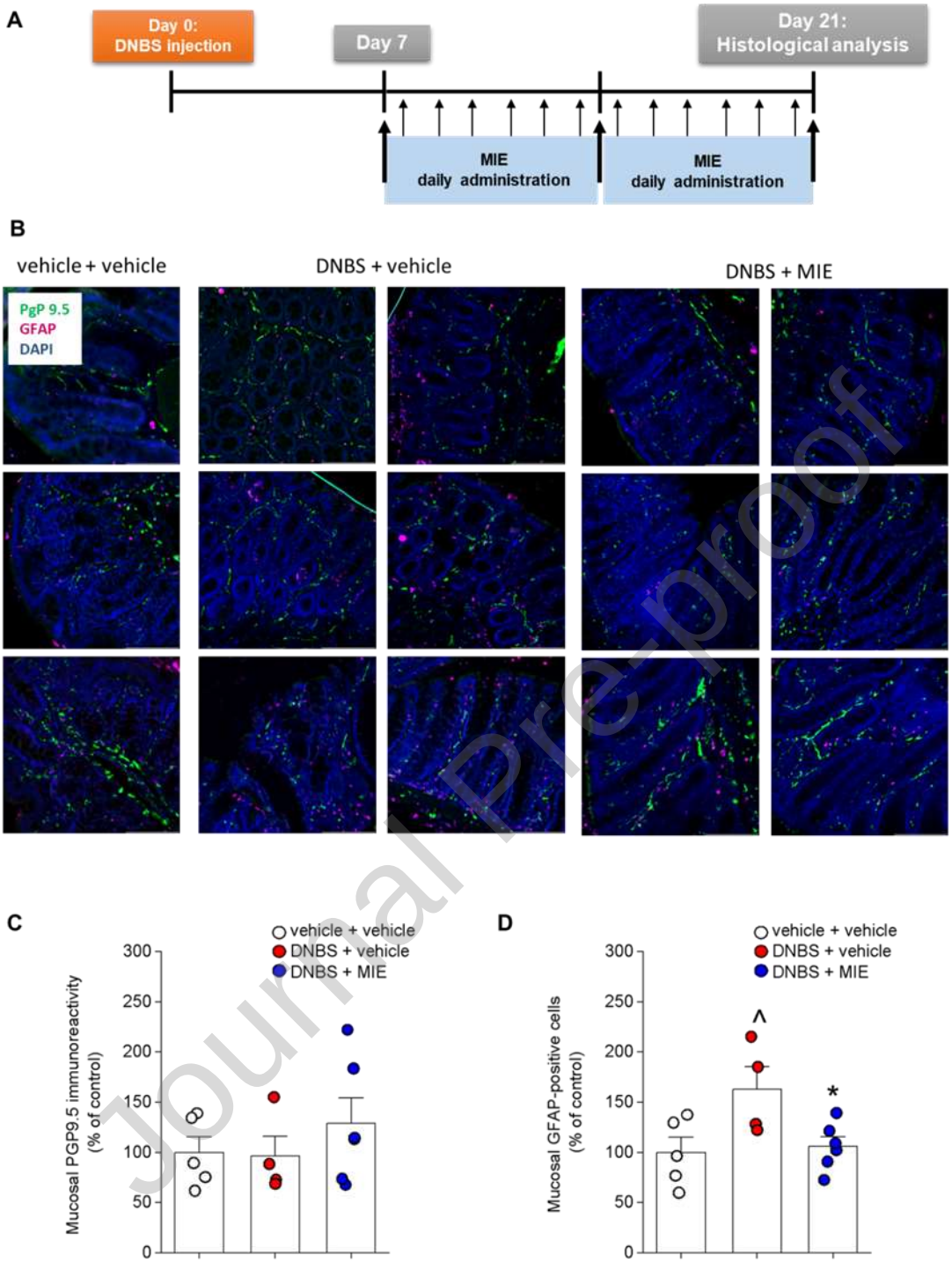

Fig. 7. MIE influence on enteric glia infiltration within the mucosa of post-colitis rats. Colitis was induced by intrarectal injection of DNBS in rats. MIE (p.o. 10 mg kg^{-1}) was administered starting from Day 7 to Day 20, representing the remission phase of colitis. On Day 21 animals were sacrificed to collect colon tissues according with the experimental scheme in **A**. The immunoreactivity of PGP9.5 (nerve endings: **C**) and the number of GFAP-positive cells (enteric glia; **D**) within the mucosa was assessed by immunofluorescence analysis on colon sections. Six to eight images (40x magnification) from the mucosa of each animal were analysed. Representative images were reported in **B**. The values represent the mean ± S.E.M. of each group (vehicle + vehicle, n=5; DNBS + vehicle, n=4; DNBS + MIE, n=6. The analysis of variance (ANOVA) was performed by one-way ANOVA with Bonferroni's significant difference procedure used for post-hoc comparisons. ^P≤0.05 *vs* vehicle + vehicle group. *P≤0.05 *vs* DNBS + vehicle group.

3.6. MIE induces a unique metabolic state in both the colon and faeces on day 21

IBD is characterized by an altered microbial composition, often referred to as dysbiosis [60]. This imbalance in the gut microbiota contributes to the recurrence of inflammation and disrupts normal metabolic processes [61]. To gain deeper insights into the effect of MIE on metabolite profiles in this *in vivo* model, we conducted a metabolomic analysis on both colon and faeces on Day 21 time point. Specifically, aqueous extracts of faecal and colonic samples from the control (vehicle + vehicle), DNBS (DNBS + vehicle), and MIE (DNBS + MIE) groups were analyzed using ^{1}H-NMR and GC-MS, respectively. Each dataset was initially analyzed independently using PCA (**Supplementary Fig. 11** and **Supplementary Fig. 12** for ^{1}H-NMR and GC-MS respectively). However, to explore potential correlations between colon and faecal metabolites and to obtain a more informative representation of samples distribution, we adopted a low-level data fusion approach. Thus, the fused data matrix was subsequently subjected to PCA. Examination of the PC1 *vs* PC2 scores plot (**Fig. 8A**) reveals a clear separation along the diagonal axis between PC1 (29.7% variance explained) and PC2 (18.2% variance explained). Specifically, MIE group (DNBS + MIE; blue triangles) were distinctly separated from the control (vehicle + vehicle) and DNBS (DNBS + vehicle) groups, indicating two key findings. First, the overlap between the control (vehicle + vehicle) and DNBS (DNBS + vehicle) groups suggests that, by Day 21, the organism has largely recovered from the DNBS-induced inflammatory state, at least at the colonic and faecal metabolomic levels. Second, MIE (DNBS + MIE) group exhibits a unique metabolic fingerprint that differentiates it from both the control (vehicle + vehicle) and DNBS (DNBS + vehicle) groups.

To elucidate the metabolic basis of this separation, we examined the loadings plot (**Fig. 8B**). In this plot, metabolites derived from colon samples are highlighted in red, while those from faecal samples are shown in green. The interpretation of the loadings plot is guided by the spatial alignment of metabolites with the respective sample clusters in the scores plot. Specifically, metabolites that increase in MIE (DNBS + MIE) group, compared to control (vehicle + vehicle) and DNBS (DNBS + vehicle) groups, are in the lower-left quadrant of the loadings plot, corresponding to the positioning of MIE samples in the scores plot (**Fig. 8A**). Conversely, metabolites that increase in control (vehicle + vehicle) and DNBS (DNBS + vehicle) groups, compared to MIE (DNBS + MIE) group, are positioned in the upper-right quadrant of the loadings plot, mirroring the spatial distribution of these samples in the scores plot.

MIE treatment in the colon increases metabolites including lysine, ornithine, tyrosine, tryptophan, succinate, and citric acid, indicating enhanced amino acid metabolism, energy production, and mitochondrial activity, in line with tissue repair and inflammation resolution. Conversely, several metabolites, including phenylalanine, glutamic acid ester, lactate, glycolic acid, mannitol, and oxalic acid, decrease, reflecting reduced glycolysis and oxidative stress. Additionally, reductions in glutamine, alanine, aspartate, and lipids like palmitic acid and stearic acid suggest a shift away from lipid metabolism and stress-induced amino acid turnover toward more efficient energy utilization. Decreases in oxoproline, hypoxanthine, and thymine indicate altered purine and pyrimidine metabolism, likely linked to improved inflammatory regulation [62]. Reduced levels of myo-inositol and ethanolamine further suggest changes in membrane remodeling and cellular signaling, supporting colonic recovery.

In faecal metabolites, MIE treatment led to an increase in galactose, acetate, and butyrate, indicating enhanced microbial fermentation and short-chain fatty acids (SCFAs) production, which are crucial for gut barrier integrity and inflammation resolution [63] though their involvement in visceral sensitivity regulation is still controversial [64]. Butyrate supports colonic epithelial health, gut barrier integrity and Treg differentiation, vital for immune homeostasis [65]. Simultaneously, several metabolites, including succinate, tryptophan, formate and various amino acids, decrease, suggesting shifts in microbial substrate utilization and host absorption. Interestingly, tryptophan was elevated in the colon, but reduced in the feces, implying enhanced host absorption and utilization, possibly for immune modulation and Treg expansion [66]. Tryptophan metabolism, leading to serotonin, kynurenine, and indole derivatives, has a central role in microbiota-host crosstalk in painful gastrointestinal disease, such as irritable bowel syndrome (IBS) and IBD [67]. The decrease in amino acids like phenylalanine, aspartate, and alanine across both compartments suggests their increased metabolic use in inflammation resolution and tissue repair. The reduced faecal succinate and formate levels, key fermentation intermediates, alongside increased acetate and butyrate, reflect a microbial shift toward beneficial SCFAs production. MIE coordinates host and microbial metabolism, as seen in the reduced phenylalanine and elevated tyrosine in the colon, indicating enhanced phenylalanine hydroxylation linked to inflammation regulation. Similarly, the decrease in faecal tryptophan, paired with increased colon levels, suggests its role in immune modulation and gut-brain axis signaling [68]. Tryptophan metabolism, essential for immune balance and influencing gut motility, pain perception, and Treg differentiation, may contribute to reducing visceral hypersensitivity in IBD. Additionally, reduced lipid and amino acid levels in both compartments suggest decreased inflammatory lipid signaling and improved metabolic efficiency. It is notable

that faecal and colon levels of histidine, the precursor to histamine, are affected by the treatment with MIE. Histamine produced by MCs, as well as by the intestinal microbiota, is indeed directly involved in visceral sensitivity regulation [37, 69]. Also, MIE effects on the levels of adenine and hypoxanthine, metabolites involved in purine salvage, may attest to a protective effect on intestinal epithelial barrier [70], though further investigations are needed to confirm this hypothesis.

Fig. 8. MIE alleviates alterations of microbiota-derived metabolites during DNBS-induced colitis. (**A**) PC1 *vs* PC2 score plot and (**B**) loading plot of the PCA model based on the combined data matrices from faecal and colon samples. Score plot legend: Control group (vehicle + vehicle; red diamonds), DNBS group (DNBS + vehicle; green squares), and MIE group (DNBS + MIE; blue triangles). Loading plot legend: faecal metabolites (green squares) and colon metabolites (red diamonds).

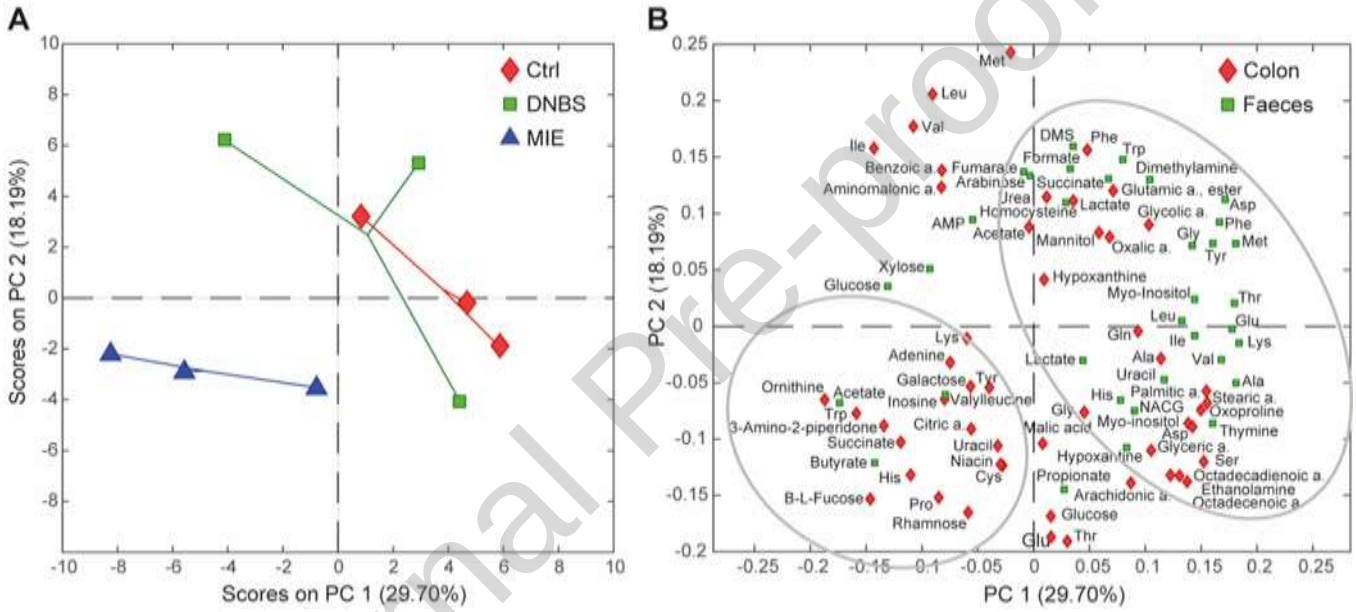

3.7. Comparative analysis of mangiferin content in endemic *Mangifera indica* cultivars and a standardized commercial extract

To conclude this study, we compared the mangiferin content of MIE, a standardized extract containing 90% mangiferin, with the mangiferin content obtained from the peel and pulp of commercial mango varieties (Keitt, Kent, and Palmer) available on the market. By analyzing their primary and secondary metabolite profiles, with a particular focus on polyphenols and mangiferin quantification, we sought to assess the potential of these local cultivars as alternative sources of this bioactive compound. Several studies have investigated the mangiferin content in various parts of *Mangifera indica* (mango) across different cultivars. For instance, research on 11 Chinese mango cultivars found that mangiferin content varied significantly among different fruit tissues. The highest concentration was detected in the peel of the Lvpimang (LPM) cultivar, with 7.49 mg g^{-1} DW, while the pulp generally contained much lower levels, often undetectable. Another study focusing on Ugandan mango leaf varieties classified them into groups based on TPC, mangiferin concentration, and antioxidant activity. Varieties in group A exhibited the highest levels of these parameters, suggesting a potential for selecting specific cultivars with superior health-promoting properties. Additionally, research comparing different fruit fractions (pulp, peel, and kernel) of two mango cultivars, Tommy Atkins and Keitt, revealed that all fractions are sources of health-promoting bioactive compounds. Regardless of cultivar, the pulp had the highest content of phytosterols (~150 mg/100 g DW), peels ranked first for pentacyclic triterpenes (from 14.2 to 17.7 mg/100 g DW), tocopherols, carotenoids, and chlorophylls, and kernels for phenolic compounds (from 421.6 to 1464.8 mg/100 g DW), flavonoids, condensed tannins, as well as hydrophilic and lipophilic antioxidant activities [71].

These studies highlight the variability in mangiferin content among different mango cultivars and plant parts, underscoring the importance of targeted analyses to identify potential sources of this bioactive compound.

Accordingly, our results revealed a significant difference in mangiferin content between the peel and pulp across the analyzed cultivars. In particular, the highest concentration was detected in the peel of ripe Keitt mango, reaching a concentration of 278.6 mg/100 g, whereas the pulp of all cultivars exhibited markedly lower levels, with values below 1 mg/100 g (**Fig. 9B**, **9E** and **9H**). These findings are consistent with previous studies indicating that mango peel represents the primary reservoir of mangiferin, whereas the pulp generally contains only trace amounts. The higher accumulation of mangiferin in the peel may be attributed to its role in plant defense mechanisms, as polyphenols, including mangiferin, are known to contribute to protection against environmental stressors, pathogens, and UV radiation. Additionally, the substantial variation in mangiferin content among different fruit parts and cultivars underscores the importance of selecting specific varieties and fruit fractions for potential nutraceutical applications. Furthermore, our analysis of phenolic acid content revealed that quinic acid was the most abundant compound detected. Once again, higher concentrations were observed in the peel compared to the pulp. In particular, the highest quinic acid content was found in the peel of unripe Palmer mango, reaching 94.3 mg/100 g (**Fig. 9G**). In contrast, the pulp of the different cultivars exhibited lower and more variable levels, ranging from 0.29 mg/100g to 1.85 mg/100 g. Based on the quantitative polyphenol profile, the cultivar with the highest total phenolic content was found to be ripe Keitt mango, in which the peel contained up to 369.73 mg/100 g of total polyphenols (**Fig. 9A** and **9B**).

In our study, we also evaluated the TPC and confirmed that the peel of ripe Keitt mango exhibited the highest polyphenol concentration, reaching 17.596 mg GAE/g. Once again, the peel displayed a significantly higher polyphenol content when compared to the pulp. The pulp samples, in fact, contained considerably lower levels of polyphenols, ranging from 0.84 mg GAE/g in Keitt pulp to 1.76 mg GAE/g in Palmer mango pulp (**Fig. 9C**, **9F** and **9I**). One of the most significant findings of this study is the predominant role of the mango peel, both ripe and unripe, in antioxidant and polyphenol content. Compared to the pulp, the peel is markedly richer in bioactive compounds, highlighting its potential value despite being commonly regarded as food waste.

Fruit ripening has a substantial impact on polyphenol concentration, particularly in the peel, where ripe mangoes exhibit higher levels of bioactive compounds and greater antioxidant activity than unripe ones. Conversely, in the pulp, an opposite trend is observed, with unripe fruits containing slightly higher concentrations of bioactive compounds than their ripe counterparts. This suggests that while ripening enhances the antioxidant properties of the peel, it leads to a decline in bioactive compound levels in the pulp.

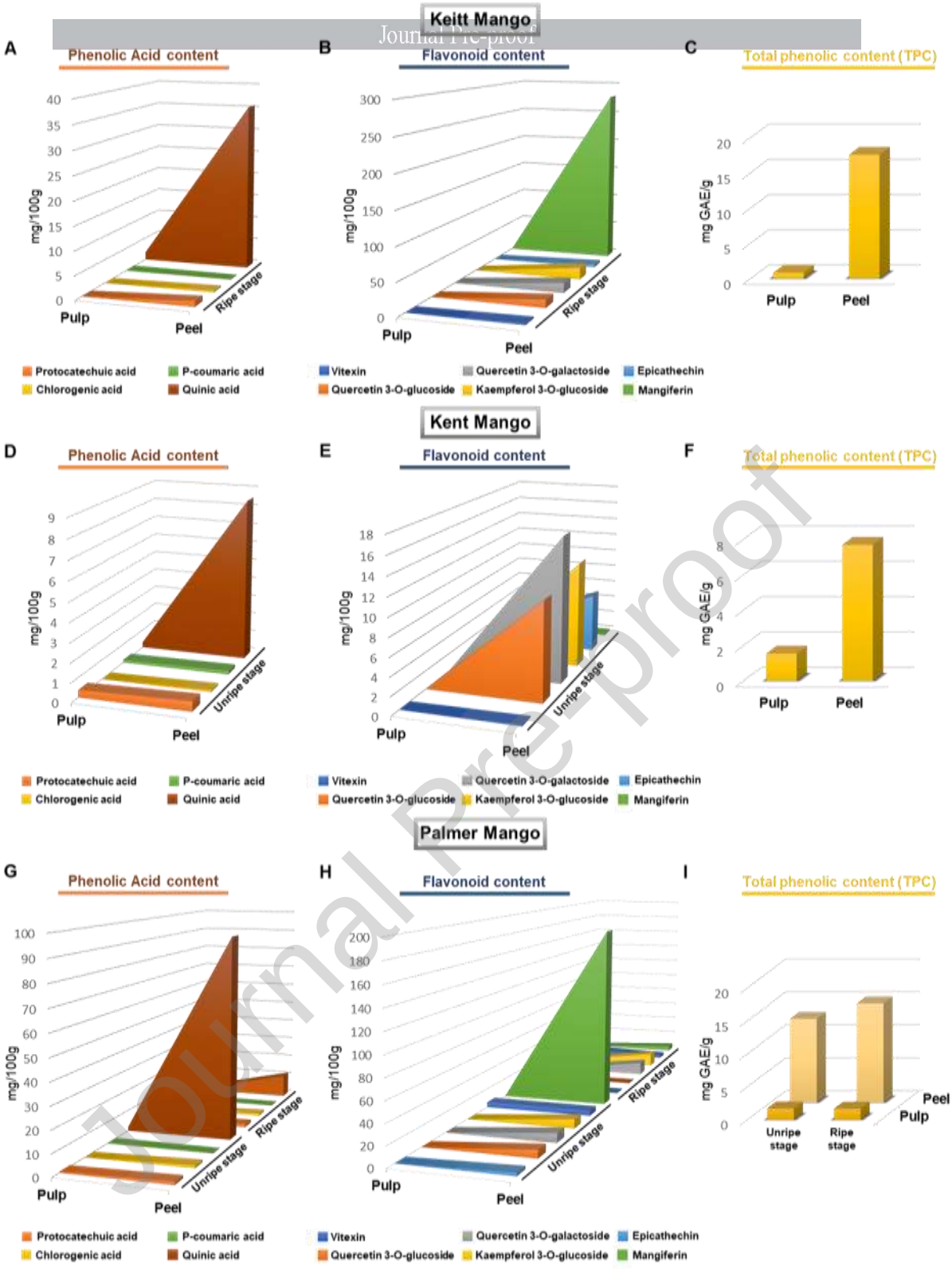

Fig. 9. Comparative analysis of mangiferin content in endemic *Mangifera indica* cultivars and a standardized commercial extract. The figure illustrates the phenolic acid content (left column, **A**, **D** and **G**), flavonoid content (middle column, **B**, **E** and **H**), and total phenolic content (TPC) (right column, **C**, **F** and **I**) in the pulp and peel of three mango varieties (Keitt, Kent, and Palmer) at different ripening stages. Analyses were conducted using UHPLC Q-Orbitrap HRMS for the quali-quantitative determination of bioactive compounds. Quinic acid, a key phenolic acid, is most abundant in the peel of ripe Keitt mango (**A**) and unripe Palmer mango (**G**). Flavonoids, such as quercetin 3-O-galactoside, are highly concentrated in the peel of unripe Kent mango (**E**) and ripe Palmer mango (**H**). Similarly, mangiferin levels are highest in the peel of ripe Keitt mango (**B**) and unripe Palmer mango (**H**). The TPC, measured using the Folin-Ciocalteu test, is significantly higher in the peel compared to the pulp across all mango varieties (**C**, **F**, **I**). These results highlight the peel as a rich source of bioactive compounds, offering potential for use in functional foods or nutraceuticals.

4. Discussion

IBD, encompassing UC and CD, represents chronic inflammatory conditions of the gastrointestinal tract that lead to substantial morbidity and significantly impair patients' quality of life. Characterized by relapsing and remitting inflammation, IBD is often accompanied by a debilitating symptomatology, which persist even during the remission phase of the disease. Chronic abdominal pain, together with gut dysmotility, is a hallmark symptom in IBD and results from complex mechanisms, including dysbiosis, peripheral and central sensitization triggered by inflammation, [72]. [73]. The multifaceted nature of visceral pain in IBD, sustained by immune and neuropathic mechanisms, makes it refractory to most pharmacological and non-pharmacological treatments. Moreover, several drugs, such as anti-inflammatory agents and pain-killers, often present limitations due to side effects and inadequate efficacy.

In this context, nutraceuticals and functional foods have garnered increasing attention as adjunctive therapeutic approaches [74]. Nutraceuticals, bioactive compounds derived from food sources, have shown promise in modulating inflammation, reducing oxidative stress, and alleviating visceral pain. Additionally, functional foods, such as prebiotics, probiotics, and polyphenol-rich foods, offer the potential to restore gut microbiota balance, enhance intestinal barrier integrity, and reduce inflammation, collectively improving IBD symptoms and overall gastrointestinal health. Incorporating nutraceuticals into IBD management presents a more integrative therapeutic approach that addresses both the inflammatory and nociceptive aspects of the disease, potentially improving patient outcomes and quality of life.

Mangifera indica L. commonly known as mango, is a rich source of bioactive compounds, with mangiferin being one of the most prominent. This xanthone glycoside is mainly concentrated in the peel and pulp of the mango fruit, as well as in its leaves and bark, and exhibits significant anti-inflammatory and immunomodulatory properties [15, 75, 76]. Previous studies in the field have shown that mango polyphenols can modulate key inflammatory pathways by the reduction of oxidative stress and the modulation of pro-inflammatory cytokines such as TNF-α, IL-6, and IL-1β in both *in vitro* and *in vivo* settings [77, 78]. Building on our recent study, which demonstrated that *Mangifera indica* L. extract (MIE, pure at 90% in mangiferin) reduced TNF-α and IL-17 levels in LPS-spiked sera from IBD patients and modulated the Th1/Th17/Treg repertoire in a T cell transfer model of colitis [13], we further expanded our investigation using an *in vivo* model of DNBS-induced colitis in rats. This experimental approach was chosen because the DNBS-induced colitis model closely replicates key features of human IBD, in terms of both response to drugs and pathophysiology, including localized inflammation, systemic immune dysregulation, epithelial barrier disruption, persistent dysbiosis and visceral hypersensitivity [16].

Our study provides compelling evidence for the therapeutic efficacy of MIE in modulating visceral pain associated with IBD, particularly focusing on its immune-modulatory effects. MIE demonstrated both symptomatic and curative efficacy against post-inflammatory visceral hypersensitivity resulting from DNBS-induced colitis. These effects were largely immune-mediated, rather than dependent on tissue repair processes, as evidenced by histological analysis showing persistent inflammatory damage in the colon despite reduced pain [35]. This suggests that MIE may represent a novel approach for managing chronic pain in IBD, especially during remission phases when pain persistence is likely driven by immune dysfunctionality among other concomitant issues. Our findings further illuminate MIE's ability to modulate both innate and adaptive immune responses during the acute and chronic phases of colitis. The involvement of neutrophils and monocytes in initiating and sustaining inflammation in IBD is well established [38]. During the acute phase of DNBS-induced colitis (Day 7), a marked increase in the infiltration of neutrophils and monocytes was observed, a hallmark of early immune response. Treatment with MIE significantly reduced the infiltration of these immune cells, particularly during the resolution phase (Day 21), demonstrating its potential to modulate the immune response and promote immune tolerance. Additionally, T-cell subsets, particularly Th1 and Th17 cells, play crucial roles in the chronic inflammation observed in IBD, contributing to disease relapses [44]. Our study revealed that MIE treatment significantly reduced the populations of both Th1 and Th17 cells, suggesting its potential to restore immune homeostasis and reduce chronic inflammation. This was further supported by a reduction in $CD4^+$ and cytotoxic $CD8^+$ T cells, indicating a broader influence on immune dynamics. The downregulation of Th1 and Th17 responses underscores MIE's ability to mitigate chronic inflammation and enhance immune regulation in IBD [13].

We also assessed the broader inflammatory milieu by measuring key cytokines and chemokines in colon tissues at both acute (Day 7) and chronic (Day 21) stages of colitis. In the acute phase, there was a marked elevation of pro-inflammatory cytokines (IL-1β, TNF-α, IL-17, IFN-γ) and chemokines (CCL2, CXCL1),

indicating active immune cell recruitment and intense inflammation [79]. While the inflammatory response had diminished on Day 21, certain mediators, such as SDF-1, TREM-1 and C5a, remained elevated, pointing to continued immune activity and possible nociceptor sensitization. MIE treatment significantly modulated the expression of these mediators, suggesting its potential to influence both the acute and chronic phases of inflammation. MIE's anti-hyperalgesic effects, particularly during the remission phase of colitis, offer a distinct therapeutic advantage in managing IBD-related pain. Despite the ongoing inflammatory damage in the colon, MIE significantly reduced visceral hypersensitivity, highlighting its immune-mediated mechanism of pain relief [80].

We further examined the role of Treg cells in regulating chronic inflammation and pain modulation in colitis. Tregs are essential for maintaining immune tolerance and regulating immune responses [49]. Our analysis revealed a significant reduction in Treg cell numbers during the acute phase of colitis (Day 7), likely due to the pro-inflammatory environment that impairs Treg function. However, on Day 21, there was a notable increase in Treg cell numbers, suggesting a compensatory mechanism to restore immune homeostasis. Interestingly, MIE treatment did not directly modulate Treg abundance, suggesting that its therapeutic effects may arise from the functional modulation of Tregs or their interactions with other immune cells [81]. Furthermore, immunofluorescence analysis showed that Treg cells were in proximity to nerve endings within the colonic mucosa. MIE treatment reduced the density of these interactions, suggesting that the treatment may influence the crosstalk between immune components and the nervous system, contributing to its anti-inflammatory and anti-hyperalgesic effects [82].

Noteworthy, MIE effects were associated with the modulation of EGCs infiltration within the mucosa. EGCs are potentially involved in several immunological disorders of the gut, including IBD, celiac disease, and autoimmune enteropathy. EGCs could directly sense invading pathogens and release pro-inflammatory cytokines such as IL-1β and IL-6. Also, enteric glia can facilitate the recruitment of lymphocytes or monocytes. Further research is warranted to elucidate the precise mechanisms underlying the crosstalk between enteric glia and immune cell subtypes, and to explore the therapeutic potential of MIE in IBDs.

In addition to its immune-modulatory effects, MIE also impacted gut microbial composition and metabolic pathways. Dysbiosis, or microbial imbalance, is frequently observed in IBD and is a significant contributor to inflammation and disease recurrence [83]. Moreover, gut dysbiosis has been demonstrated to be a driver of pain chronicity in the DNBS-model of colitis [12]. Metabolomic analysis of colon and fecal samples revealed distinct metabolic shifts in the MIE-treated group, highlighting alterations in both host metabolism and gut microbial activity. MIE treatment promoted the production of metabolites such as lysine, ornithine, tryptophan, succinate, and citric acid, indicative of enhanced amino acid metabolism and mitochondrial activity, both of which are associated with inflammation resolution [84]. Additionally, increased levels of SCFAs like butyrate and acetate in the faeces suggest that MIE promotes microbial fermentation and gut barrier integrity, both essential for resolving inflammation. The altered tryptophan metabolism observed in both the colon and faeces also suggests a potential mechanism for immune modulation and Treg expansion and pain regulation.

Of note, this study highlights the untapped potential of mango peel, traditionally considered waste, as a valuable source of bioactive compounds with substantial nutraceutical applications. Our analysis demonstrates that mango peel, particularly from ripe Keitt mangoes, contains significantly higher concentrations of bioactive compounds such as mangiferin and polyphenols compared to the pulp. This suggests that mango peel could be harnessed as a sustainable, natural resource for bioactive ingredients with therapeutic potential [85]. The targeted metabolomic approach applied in this study not only provides a robust chemical fingerprint of these cultivars but also establishes a crucial foundation for the potential pharmacological and nutraceutical translatability of our findings. Given the increasing interest in plant-derived bioactives for functional food development and therapeutic applications, our results underline the necessity of implementing rigorous agrifood quality control measures for local cultivars.

5. Conclusion and study limitation

Managing chronic pain in patients with IBD remains a significant challenge. IBD is driven by immune dysregulation, primarily involving Th1 and Th17 cells, and sustained by pro-inflammatory cytokines and chemokines. This inflammatory milieu often results in persistent visceral pain, which can continue even after intestinal damage has healed and is frequently resistant to conventional anti-inflammatory treatments. Our

study investigated the potential therapeutic effects of *Mangifera indica* L. extract (MIE), rich in mangiferin, on both gut inflammation and visceral pain in a DNBS-induced rat model of colitis. Our findings demonstrated that acute MIE administration effectively and dose-dependently alleviated post-inflammatory visceral pain in DNBS-treated rats. Moreover, repeated MIE administration prevented the persistence of pain during the remission phase. MIE also significantly reduced Th1 and Th17 cell infiltration, monocyte influx, and levels of key pro-inflammatory cytokines (IL-1β, TNF-α) and chemokines (CXCL1, CXCL2). While the histopathological analysis did not reveal significant tissue healing, MIE modulated interactions between Treg cells and nerve endings in the colonic mucosa, leading to a reduction in surrounding glial cells. Additionally, MIE administration was associated with the restoration of SCFAs (acetate and butyrate) in faecal samples.

These findings suggest that MIE holds promise as a dual-action therapeutic approach, potentially serving as a complementary or adjuvant therapy for IBD by targeting both inflammatory pathways and chronic visceral pain, the latter is still an unmet need in clinical practise [86]. However, several limitations must be considered. First, our study was conducted in a DNBS-induced colitis rat model, which, although sharing key pathological features with human IBD, does not fully replicate its complexity, including genetic susceptibility and environmental triggers. The differences between rodent and human immune responses may limit direct clinical translation. Another limitation to the generalisability of our findings is the lack of consideration for gender and sex-related factors, which may influence both disease progression and treatment response. Second, the specific molecular mechanisms underlying MIE effects remain incompletely understood. A plethora of mechanisms have been proposed to be responsible for pain-relieving properties of mangiferin in other pathological conditions, including modulation of opioid, purine and α2 adrenergic receptors signalling and several proteins involved in sensitivity regulation have been predicted to bind mangiferin [87, 88]. While our study demonstrated immune modulation and SCFAs restoration, additional research is needed to clarify the precise signaling pathways mainly involved in MIE anti-hyperalgesic effects. To this end, it is necessary to further clarify the relationship between post-inflammatory immune derangement and the persistence of pain. However, considering the complex nature of pain associated with IBD, which displays inflammatory, neuropathic and microbial components [16], it is reasonable to think that MIE efficacy on pain is the result of multiple mechanisms. Third, the bioavailability and pharmacokinetics of MIE in humans require further investigation. While our results suggest beneficial effects in rodents, the absorption, metabolism, and optimal dosing in human subjects remain unknown. Variability in gut microbiota composition may also influence MIE's therapeutic efficacy. Fourth, potential side effects or long-term safety concerns were not addressed in this study. Although MIE appeared well-tolerated in our animal model, possible adverse effects in humans, particularly with prolonged use, need to be evaluated in clinical trials. Finally, while our study focused on MIE anti-inflammatory and analgesic properties, its interactions with existing IBD treatments remain unexplored. Future research should assess whether MIE could enhance or interfere with standard therapies such as biologics, immunosuppressants, or dietary interventions.

In conclusion, while our findings support the therapeutic potential of MIE in IBD, including pain management, further clinical studies are essential to confirm its efficacy, safety, and long-term benefits in human patients. Additionally, this study highlights the potential for future research into the optimization of cultivation practices aimed at maximizing the bioactive compound yield, thereby reinforcing the role of endemic *Mangifera indica* cultivars as promising candidates for nutraceuticals and/or functional food innovation and sustainable agricultural exploitation.

Author contributions. Elena Lucarini: Conceptualization, Data curation, Formal analysis, Investigation, Methodology, Visualization, Writing – original draft. **Anna Schettino:** Conceptualization, Data curation, Formal analysis, Investigation, Methodology, Visualization, Writing – original draft. **Noemi Marigliano:** Data curation, Formal analysis, Investigation. **Clara Ciampi:** Data curation, Investigation. **Martina Smimmo:** Data curation, Investigation. **Francesca Romano:** Data curation, Investigation. **Antonio Paolillo:** Data curation, Investigation. **Luana Izzo:** Data curation, Investigation, Investigation, Visualization. **Jenefa Begum:** Data curation, Investigation. **Adel Abo Mansour:** Data curation, Investigation. **Nunzia Iaccarino:** Data curation, Investigation, Visualization. **Antonio Randazzo:** Writing – original draft. **Karin Vicente Greco:** Writing – original draft. **Raffaele Scarpa:** Writing – original draft, Visulalization. **Francesco Caso:** Writing – original draft, Visualization. **Asif Jilani Iqbal:** Writing – original draft, Writing – review & editing. **Mariarosaria Bucci:** Writing – original draft. **Carla Ghelardini:** Writing – original draft. **Lorenzo Di Cesare Mannelli:** Project administration, Supervision, Writing – original draft, Writing – review & editing. **Anella Saviano:** Conceptualization, Data curation, Investigation, Writing – original draft, Writing – review & editing. **Francesco Maione:** Project administration, Supervision, Writing – original draft, Writing – review & editing.

Funding and acknowledgements. This study was supported by internal funding from the *ImmunoPharmaLab*, Department of Pharmacy, University of Naples, Federico II. ASav is supported by RTD-A research contract for the thematic spoke "Validating acid nucleic-based drugs using in vitro and in vivo models of cancer and immune-related diseases". The research activity is focused on topics of interest for the Department of Pharmacy, Federico II, included in the grant application marked MUR identification code CN00000041 "National Center for Gene Therapy and Drugs based on RNA Technology" (initiative financed by the European Union – NextGenerationEU and Funding granted with Directorial Decree n.1035 of 06.17.2022 under PNRR MUR – M4C2 – Investment 1.4- CUP UNINA: E63C22000940007). AJI Supported BHF Project grant PG/23/11476. AAM extends his appreciation to the Deanship of Research and Graduate Studies at King Khalid University for funding via small group research project under grant number RGP1/122/45. NM is supported by AORN A. Cardarelli Scholarship (n. 725/2022 GRC- Linea Progettuale 1.3: "Gestione delle cronicità"). ASch is supported by University of Naples Federico II PhD scholarship in "Nutraceuticals, functional foods and human health" (PNRR DM 118 M4C1– INV 4.1 ricerca PNRR generici). CG and LDCM are supported by the Italian Ministry of Instruction, University and Research and by the University of Florence.

Data, materials and software availability. All data associated with this study are present in the paper or the online supplemental materials. Requests for reagents should be directed to the corresponding author and will be made available after completion of a material transfer agreement with *ImmunoPharmaLab*, Department of Pharmacy, University of Naples Federico II and/or NEUROFARBA, Department of Neuroscience, University of Florence

References

[1] D.K. Podolsky, Inflammatory bowel disease, N. Engl. J. Med. 347(6) (2002) 417-29.
[2] N. Bakshi, A.L. Hart, M.C. Lee, A.C.C. Williams, J.M. Lackner, C. Norton, P. Croft, Chronic pain in patients with inflammatory bowel disease, Pain 162(10) (2021) 2466-2471.
[3] A. Kaser, S. Zeissig, R.S. Blumberg, Inflammatory bowel disease, Annu. Rev. Immunol. 28 (2010) 573-621.
[4] M.F. Neurath, Cytokines in inflammatory bowel disease, Nat. Rev. Immunol. 14(5) (2014) 329-42.
[5] M.G. Neuman, Immune dysfunction in inflammatory bowel disease, Transl. Res. 149(4) (2007) 173-86.
[6] E.A. Mayer, K. Tillisch, The brain-gut axis in abdominal pain syndromes, Annu. Rev. Med. 62 (2011) 381-96.
[7] L. Grundy, A. Erickson, S.M. Brierley, Visceral Pain, Annu Rev Physiol 81 (2019) 261-284.
[8] E.A. Mayer, B.D. Naliboff, A.D. Craig, Neuroimaging of the brain-gut axis: from basic understanding to treatment of functional GI disorders, Gastroenterology 131(6) (2006) 1925-42.
[9] C. Günther, V. Rothhammer, M. Karow, M. Neurath, B. Winner, The Gut-Brain Axis in Inflammatory Bowel Disease-Current and Future Perspectives, Int. J. Mol. Sci. 22(16) (2021).
[10] L. Ge, S. Liu, S. Li, J. Yang, G. Hu, C. Xu, W. Song, Psychological stress in inflammatory bowel disease: Psychoneuroimmunological insights into bidirectional gut-brain communications, Front. Immunol. 13 (2022) 1016578.
[11] L.M. Genaro, L.E.M. Gomes, A. Franceschini, H.D. Ceccato, R.N. de Jesus, A.P. Lima, C.K. Nagasako, J.J. Fagundes, M.L.S. Ayrizono, R.F. Leal, Anti-TNF therapy and immunogenicity in inflammatory bowel diseases: a translational approach, Am J Transl Res 13(12) (2021) 13916-13930.
[12] E. Lucarini, V. Di Pilato, C. Parisio, L. Micheli, A. Toti, A. Pacini, G. Bartolucci, S. Baldi, E. Niccolai, A. Amedei, G.M. Rossolini, C. Nicoletti, J.F. Cryan, S.M. O'Mahony, C. Ghelardini, L. Di Cesare Mannelli, Visceral sensitivity modulation by faecal microbiota transplantation: the active role of gut bacteria in pain persistence, Pain 163(5) (2022) 861-877.
[13] A. Saviano, A. Schettino, N. Iaccarino, A.A. Mansour, J. Begum, N. Marigliano, F. Raucci, F. Romano, G. Riccardi, E. Mitidieri, R. d'Emmanuele di Villa Bianca, I. Bello, E. Panza, M. Smimmo, V. Vellecco, P. Rimmer, J. Cheesbrough, Z. Zhi, T.H. Iqbal, S. Pieretti, V.M. D'Amore, L. Marinelli, V. La Pietra, R. Sorrentino, L. Costa, F. Caso, R. Scarpa, G. Cirino, A. Randazzo, M. Bucci, H.M. McGettrick, A.J. Iqbal, F. Maione, A reverse translational approach reveals the protective roles of Mangifera indica in inflammatory bowel disease, J. Autoimmun. 144 (2024) 103181.
[14] H. Kim, N. Banerjee, R.C. Barnes, C.M. Pfent, S.T. Talcott, R.H. Dashwood, S.U. Mertens-Talcott, Mango polyphenolics reduce inflammation in intestinal colitis-involvement of the miR-126/PI3K/AKT/mTOR axis in vitro and in vivo, Mol. Carcinog. 56(1) (2017) 197-207.
[15] A. Saviano, F. Raucci, G.M. Casillo, A.A. Mansour, V. Piccolo, C. Montesano, M. Smimmo, V. Vellecco, G. Capasso, A. Boscaino, V. Summa, N. Mascolo, A.J. Iqbal, R. Sorrentino, R. d'Emmanuele di Villa Bianca, M. Bucci, V. Brancaleone, F. Maione, Anti-inflammatory and immunomodulatory activity of Mangifera indica L. reveals the modulation of COX-2/mPGES-1 axis and Th17/Treg ratio, Pharmacol. Res. 182 (2022) 106283.

[16] E. Lucarini, C. Parisio, J.J.V. Branca, C. Segnani, C. Ippolito, C. Pellegrini, L. Antonioli, M. Fornai, L. Micheli, A. Pacini, N. Bernardini, C. Blandizzi, C. Ghelardini, L. Di Cesare Mannelli, Deepening the Mechanisms of Visceral Pain Persistence: An Evaluation of the Gut-Spinal Cord Relationship, Cells 9(8) (2020).
[17] M. Colucci, F. Maione, M.C. Bonito, A. Piscopo, A. Di Giannuario, S. Pieretti, New insights of dimethyl sulphoxide effects (DMSO) on experimental in vivo models of nociception and inflammation, Pharmacol. Res. 57(6) (2008) 419-25.
[18] K. Forster, A. Goethel, C.W. Chan, G. Zanello, C. Streutker, K. Croitoru, An oral CD3-specific antibody suppresses T-cell-induced colitis and alters cytokine responses to T-cell activation in mice, Gastroenterology 143(5) (2012) 1298-1307.
[19] M.Y. Song, C.P. Hong, S.J. Park, J.H. Kim, B.G. Yang, Y. Park, S.W. Kim, K.S. Kim, J.Y. Lee, S.W. Lee, M.H. Jang, Y.C. Sung, Protective effects of Fc-fused PD-L1 on two different animal models of colitis, Gut 64(2) (2015) 260-71.
[20] H. Li, Y. Zhang, M. Liu, C. Fan, C. Feng, Q. Lu, C. Xiang, H. Lu, X. Yang, B. Wu, D. Zou, W. Tang, Targeting PDE4 as a promising therapeutic strategy in chronic ulcerative colitis through modulating mucosal homeostasis, Acta Pharm Sin B 12(1) (2022) 228-245.
[21] K. Shimizu, K. Agata, S. Takasugi, S. Goto, Y. Narita, T. Asai, Y. Magata, N. Oku, New strategy for MS treatment with autoantigen-modified liposomes and their therapeutic effect, J. Control. Release 335 (2021) 389-397.
[22] H. Li, C. Fan, H. Lu, C. Feng, P. He, X. Yang, C. Xiang, J. Zuo, W. Tang, Protective role of berberine on ulcerative colitis through modulating enteric glial cells-intestinal epithelial cells-immune cells interactions, Acta Pharm Sin B 10(3) (2020) 447-461.
[23] A. Cossarizza, H.D. Chang, A. Radbruch, S. Abrignani, R. Addo, M. Akdis, I. Andrä, F. Andreata, F. Annunziato, E. Arranz, P. Bacher, S. Bari, V. Barnaba, J. Barros-Martins, D. Baumjohann, C.G. Beccaria, D. Bernardo, D.A. Boardman, J. Borger, C. Böttcher, L. Brockmann, M. Burns, D.H. Busch, G. Cameron, I. Cammarata, A. Cassotta, Y. Chang, F.G. Chirdo, E. Christakou, L. Čičin-Šain, L. Cook, A.J. Corbett, R. Cornelis, L. Cosmi, M.S. Davey, S. De Biasi, G. De Simone, G. Del Zotto, M. Delacher, F. Di Rosa, J. Di Santo, A. Diefenbach, J. Dong, T. Dörner, R.J. Dress, C.A. Dutertre, S.B.G. Eckle, P. Eede, M. Evrard, C.S. Falk, M. Feuerer, S. Fillatreau, A. Fiz-Lopez, M. Follo, G.A. Foulds, J. Fröbel, N. Gagliani, G. Galletti, A. Gangaev, N. Garbi, J.A. Garrote, J. Geginat, N.A. Gherardin, L. Gibellini, F. Ginhoux, D.I. Godfrey, P. Gruarin, C. Haftmann, L. Hansmann, C.M. Harpur, A.C. Hayday, G. Heine, D.C. Hernández, M. Herrmann, O. Hoelsken, Q. Huang, S. Huber, J.E. Huber, J. Huehn, M. Hundemer, W.Y.K. Hwang, M. Iannacone, S.M. Ivison, H.M. Jäck, P.K. Jani, B. Keller, N. Kessler, S. Ketelaars, L. Knop, J. Knopf, H.F. Koay, K. Kobow, K. Kriegsmann, H. Kristyanto, A. Krueger, J.F. Kuehne, H. Kunze-Schumacher, P. Kvistborg, I. Kwok, D. Latorre, D. Lenz, M.K. Levings, A.C. Lino, F. Liotta, H.M. Long, E. Lugli, K.N. MacDonald, L. Maggi, M.K. Maini, F. Mair, C. Manta, R.A. Manz, M.F. Mashreghi, A. Mazzoni, J. McCluskey, H.E. Mei, F. Melchers, S. Melzer, D. Mielenz, L. Monin, L. Moretta, G. Multhoff, L.E. Muñoz, M. Muñoz-Ruiz, F. Muscate, A. Natalini, K. Neumann, L.G. Ng, A. Niedobitek, J. Niemz, L.N. Almeida, S. Notarbartolo, L. Ostendorf, L.J. Pallett, A.A. Patel, G.I. Percin, G. Peruzzi, M. Pinti, A.G. Pockley, K. Pracht, I. Prinz, I. Pujol-Autonell, N. Pulvirenti, L. Quatrini, K.M. Quinn, H. Radbruch, H. Rhys, M.B. Rodrigo, C. Romagnani, C. Saggau, S. Sakaguchi, F. Sallusto, L. Sanderink, I. Sandrock, C. Schauer, A. Scheffold, H.U. Scherer, M. Schiemann, F.A. Schildberg, K. Schober, J. Schoen, W. Schuh, T. Schüler, A.R. Schulz, S. Schulz, J. Schulze, S. Simonetti, J. Singh, K.M. Sitnik, R. Stark, S. Starossom, C. Stehle, F. Szelinski, L. Tan, A. Tarnok, J. Tornack, T.I.M. Tree, J.J.P. van Beek, W. van de Veen, K. van Gisbergen, C. Vasco, N.A. Verheyden, A. von Borstel, K.A. Ward-Hartstonge, K. Warnatz, C. Waskow, A. Wiedemann, A. Wilharm, J. Wing, O. Wirz, J. Wittner, J.H.M. Yang, J. Yang, Guidelines for the use of flow cytometry and cell sorting in immunological studies (third edition), Eur J Immunol 51(12) (2021) 2708-3145.
[24] M. Cui, A. Trimigno, V. Aru, B. Khakimov, S.B. Engelsen, Human Faecal (1)H NMR Metabolomics: Evaluation of Solvent and Sample Processing on Coverage and Reproducibility of Signature Metabolites, Anal. Chem. 92(14) (2020) 9546-9555.
[25] Y.S. Hong, Y.T. Ahn, J.C. Park, J.H. Lee, H. Lee, C.S. Huh, D.H. Kim, D.H. Ryu, G.S. Hwang, 1H NMR-based metabonomic assessment of probiotic effects in a colitis mouse model, Arch. Pharm. Res. 33(7) (2010) 1091-101.
[26] N. Iaccarino, J. Amato, B. Pagano, A. Di Porzio, M. Micucci, L. Bolelli, R. Aldini, E. Novellino, R. Budriesi, A. Randazzo, Impact of phytosterols on liver and distal colon metabolome in experimental murine colitis model: an explorative study, J Enzyme Inhib Med Chem 34(1) (2019) 1041-1050.
[27] F. Romano, E. Di Gregorio, G. Riccardi, C. Furlan, N. Cavallini, F. Savorani, A. Di Porzio, S. De Tito, A. Randazzo, E. Gianolio, N. Iaccarino, Comparison of the biological effects of gadodiamide (Omniscan) and gadoteridol (ProHance) by means of multi-organ and plasma metabolomics, Analyst 148(11) (2023) 2415-2424.
[28] F. Savorani, G. Tomasi, S.B. Engelsen, icoshift: A versatile tool for the rapid alignment of 1D NMR spectra, J. Magn. Reson. 202(2) (2010) 190-202.
[29] M. Mafata, J. Brand, M. Kidd, A. Medvedovici, A. Buica, Exploration of Data Fusion Strategies Using Principal Component Analysis and Multiple Factor Analysis, Beverages 8 (2022) 66.
[30] C. Cristiano, F. Volpicelli, P. Lippiello, B. Buono, F. Raucci, M. Piccolo, A.J. Iqbal, C. Irace, M.C. Miniaci, C. Perrone Capano, A. Calignano, N. Mascolo, F. Maione, Neutralization of IL-17 rescues amyloid-β-induced neuroinflammation and memory impairment, Br J Pharmacol 176(18) (2019) 3544-3557.

[31] E. Lucarini, L. Micheli, A. Toti, C. Ciampi, F. Margiotta, L. Di Cesare Mannelli, C. Ghelardini, Anti-Hyperalgesic Efficacy of Acetyl L-Carnitine (ALCAR) Against Visceral Pain Induced by Colitis: Involvement of Glia in the Enteric and Central Nervous System, Int. J. Mol. Sci. 24(19) (2023).
[32] G.A. Ojeda, S.C. Sgroppo, C. Sánchez-Moreno, B. de Ancos, Mango 'criollo' by-products as a source of polyphenols with antioxidant capacity. Ultrasound assisted extraction evaluated by response surface methodology and HPLC-ESI-QTOF-MS/MS characterization, Food Chem. 396 (2022) 133738.
[33] L. Izzo, L. Castaldo, S. Lombardi, A. Gaspari, M. Grosso, A. Ritieni, Bioaccessibility and Antioxidant Capacity of Bioactive Compounds From Various Typologies of Canned Tomatoes, Front Nutr 9 (2022) 849163.
[34] L. Castaldo, L. Izzo, A. Narváez, Y. Rodríguez-Carrasco, M. Grosso, A. Ritieni, Colon Bioaccessibility under In Vitro Gastrointestinal Digestion of Different Coffee Brews Chemically Profiled through UHPLC-Q-Orbitrap HRMS, Foods 10(1) (2021).
[35] G.T. Ho, J.A. Cartwright, E.J. Thompson, C.C. Bain, A.G. Rossi, Resolution of Inflammation and Gut Repair in IBD: Translational Steps Towards Complete Mucosal Healing, Inflamm. Bowel Dis. 26(8) (2020) 1131-1143.
[36] J. Aguilera-Lizarraga, M. Florens, H. Hussein, G. Boeckxstaens, Local immune response as novel disease mechanism underlying abdominal pain in patients with irritable bowel syndrome, Acta Clin. Belg. 77(5) (2022) 889-896.
[37] J. Aguilera-Lizarraga, M.V. Florens, M.F. Viola, P. Jain, L. Decraecker, I. Appeltans, M. Cuende-Estevez, N. Fabre, K. Van Beek, E. Perna, D. Balemans, N. Stakenborg, S. Theofanous, G. Bosmans, S.U. Mondelaers, G. Matteoli, S. Ibiza Martínez, C. Lopez-Lopez, J. Jaramillo-Polanco, K. Talavera, Y.A. Alpizar, T.B. Feyerabend, H.R. Rodewald, R. Farre, F.A. Redegeld, J. Si, J. Raes, C. Breynaert, R. Schrijvers, C. Bosteels, B.N. Lambrecht, S.D. Boyd, R.A. Hoh, D. Cabooter, M. Nelis, P. Augustijns, S. Hendrix, J. Strid, R. Bisschops, D.E. Reed, S.J. Vanner, A. Denadai-Souza, M.M. Wouters, G.E. Boeckxstaens, Local immune response to food antigens drives meal-induced abdominal pain, Nature 590(7844) (2021) 151-156.
[38] B.M. Fournier, C.A. Parkos, The role of neutrophils during intestinal inflammation, Mucosal Immunol. 5(4) (2012) 354-66.
[39] A. Mantovani, M.A. Cassatella, C. Costantini, S. Jaillon, Neutrophils in the activation and regulation of innate and adaptive immunity, Nat. Rev. Immunol. 11(8) (2011) 519-31.
[40] N. Borregaard, Neutrophils, from marrow to microbes, Immunity 33(5) (2010) 657-70.
[41] B. Amulic, C. Cazalet, G.L. Hayes, K.D. Metzler, A. Zychlinsky, Neutrophil function: from mechanisms to disease, Annu. Rev. Immunol. 30 (2012) 459-89.
[42] C. Shi, E.G. Pamer, Monocyte recruitment during infection and inflammation, Nat. Rev. Immunol. 11(11) (2011) 762-74.
[43] I. Tindemans, M.E. Joosse, J.N. Samsom, Dissecting the Heterogeneity in T-Cell Mediated Inflammation in IBD, Cells 9(1) (2020).
[44] T. Kobayashi, S. Okamoto, T. Hisamatsu, N. Kamada, H. Chinen, R. Saito, M.T. Kitazume, A. Nakazawa, A. Sugita, K. Koganei, K. Isobe, T. Hibi, IL23 differentially regulates the Th1/Th17 balance in ulcerative colitis and Crohn's disease, Gut 57(12) (2008) 1682-9.
[45] M.F. Neurath, Strategies for targeting cytokines in inflammatory bowel disease, Nat. Rev. Immunol. 24(8) (2024) 559-576.
[46] D. Aebisher, D. Bartusik-Aebisher, A. Przygórzewska, P. Oleś, P. Woźnicki, A. Kawczyk-Krupka, Key Interleukins in Inflammatory Bowel Disease-A Review of Recent Studies, Int. J. Mol. Sci. 26(1) (2024).
[47] D. Wang, R.N. Dubois, A. Richmond, The role of chemokines in intestinal inflammation and cancer, Curr. Opin. Pharmacol. 9(6) (2009) 688-96.
[48] J.M. Zhang, J. An, Cytokines, inflammation, and pain, Int. Anesthesiol. Clin. 45(2) (2007) 27-37.
[49] M. Laukova, A. Glatman Zaretsky, Regulatory T cells as a therapeutic approach for inflammatory bowel disease, Eur J Immunol 53(2) (2023) e2250007.
[50] K.R. Charley, A.G. Ramstead, J.G. Matous, Y. Kumaki, L.M. Sircy, J.S. Hale, M.A. Williams, Effector-Phase IL-2 Signals Drive Th1 Effector and Memory Responses Dependently and Independently of TCF-1, J Immunol 212(4) (2024) 586-595.
[51] S. Swaroop, N. Sengupta, A.R. Suryawanshi, Y.K. Adlakha, A. Basu, HSP60 plays a regulatory role in IL-1β-induced microglial inflammation via TLR4-p38 MAPK axis, J. Neuroinflammation 13 (2016) 27.
[52] W. van Eden, R. van der Zee, B. Prakken, Heat-shock proteins induce T-cell regulation of chronic inflammation, Nat. Rev. Immunol. 5(4) (2005) 318-30.
[53] S. Hori, T. Nomura, S. Sakaguchi, Control of regulatory T cell development by the transcription factor Foxp3, Science 299(5609) (2003) 1057-61.
[54] J.D. Fontenot, M.A. Gavin, A.Y. Rudensky, Foxp3 programs the development and function of CD4+CD25+ regulatory T cells, Nat. Immunol. 4(4) (2003) 330-6.
[55] S.Z. Josefowicz, A. Rudensky, Control of regulatory T cell lineage commitment and maintenance, Immunity 30(5) (2009) 616-25.

[56] S. Negi, S. Saini, N. Tandel, K. Sahu, R.P.N. Mishra, R.K. Tyagi, Translating Treg Therapy for Inflammatory Bowel Disease in Humanized Mice, Cells 10(8) (2021).
[57] L. Seguella, B.D. Gulbransen, Enteric glial biology, intercellular signalling and roles in gastrointestinal disease, Nat. Rev. Gastroenterol. Hepatol. 18(8) (2021) 571-587.
[58] V. Grubišić, J.L. McClain, D.E. Fried, I. Grants, P. Rajasekhar, E. Csizmadia, O.A. Ajijola, R.E. Watson, D.P. Poole, S.C. Robson, F.L. Christofi, B.D. Gulbransen, Enteric Glia Modulate Macrophage Phenotype and Visceral Sensitivity following Inflammation, Cell Rep. 32(10) (2020) 108100.
[59] F. Progatzky, M. Shapiro, S.H. Chng, B. Garcia-Cassani, C.H. Classon, S. Sevgi, A. Laddach, A.C. Bon-Frauches, R. Lasrado, M. Rahim, E.M. Amaniti, S. Boeing, K. Shah, L.J. Entwistle, A. Suárez-Bonnet, M.S. Wilson, B. Stockinger, V. Pachnis, Regulation of intestinal immunity and tissue repair by enteric glia, Nature 599(7883) (2021) 125-130.
[60] Q. Meng, J. Guo, K. Lv, Y. Liu, J. Zhang, M. Li, X. Cheng, S. Chen, X. Huo, Q. Zhang, Y. Chen, J. Li, 5S-Heudelotinone alleviates experimental colitis by shaping the immune system and enhancing the intestinal barrier in a gut microbiota-dependent manner, Acta Pharm Sin B 14(5) (2024) 2153-2176.
[61] S. Deleu, K. Machiels, J. Raes, K. Verbeke, S. Vermeire, Short chain fatty acids and its producing organisms: An overlooked therapy for IBD?, EBioMedicine 66 (2021) 103293.
[62] J.S. Lee, R.X. Wang, E.E. Alexeev, J.M. Lanis, K.D. Battista, L.E. Glover, S.P. Colgan, Hypoxanthine is a checkpoint stress metabolite in colonic epithelial energy modulation and barrier function, J Biol Chem 293(16) (2018) 6039-6051.
[63] M.A. Vinolo, H.G. Rodrigues, R.T. Nachbar, R. Curi, Regulation of inflammation by short chain fatty acids, Nutrients 3(10) (2011) 858-76.
[64] I.A.M. van Thiel, S. Botschuijver, W.J. de Jonge, J. Seppen, Painful interactions: Microbial compounds and visceral pain, Biochim Biophys Acta Mol Basis Dis 1866(1) (2020) 165534.
[65] Y. Furusawa, Y. Obata, S. Fukuda, T.A. Endo, G. Nakato, D. Takahashi, Y. Nakanishi, C. Uetake, K. Kato, T. Kato, M. Takahashi, N.N. Fukuda, S. Murakami, E. Miyauchi, S. Hino, K. Atarashi, S. Onawa, Y. Fujimura, T. Lockett, J.M. Clarke, D.L. Topping, M. Tomita, S. Hori, O. Ohara, T. Morita, H. Koseki, J. Kikuchi, K. Honda, K. Hase, H. Ohno, Commensal microbe-derived butyrate induces the differentiation of colonic regulatory T cells, Nature 504(7480) (2013) 446-50.
[66] C. Michaudel, C. Danne, A. Agus, A. Magniez, A. Aucouturier, M. Spatz, A. Lefevre, J. Kirchgesner, N. Rolhion, Y. Wang, A. Lavelle, C. Galbert, G. Da Costa, M. Poirier, A. Lapière, J. Planchais, P. Nádvorník, P. Illes, C. Oeuvray, L. Creusot, M.L. Michel, N. Benech, A. Bourrier, I. Nion-Larmurier, C. Landman, M.L. Richard, P. Emond, P. Seksik, L. Beaugerie, R.R. Arguello, D. Moulin, S. Mani, Z. Dvorák, L.G. Bermúdez-Humarán, P. Langella, H. Sokol, Rewiring the altered tryptophan metabolism as a novel therapeutic strategy in inflammatory bowel diseases, Gut 72(7) (2023) 1296-1307.
[67] A. Agus, J. Planchais, H. Sokol, Gut Microbiota Regulation of Tryptophan Metabolism in Health and Disease, Cell Host Microbe 23(6) (2018) 716-724.
[68] K. Gao, C.L. Mu, A. Farzi, W.Y. Zhu, Tryptophan Metabolism: A Link Between the Gut Microbiota and Brain, Adv. Nutr. 11(3) (2020) 709-723.
[69] G. De Palma, C. Shimbori, D.E. Reed, Y. Yu, V. Rabbia, J. Lu, N. Jimenez-Vargas, J. Sessenwein, C. Lopez-Lopez, M. Pigrau, J. Jaramillo-Polanco, Y. Zhang, L. Baerg, A. Manzar, J. Pujo, X. Bai, M.I. Pinto-Sanchez, A. Caminero, K. Madsen, M.G. Surette, M. Beyak, A.E. Lomax, E.F. Verdu, S.M. Collins, S.J. Vanner, P. Bercik, Histamine production by the gut microbiota induces visceral hyperalgesia through histamine 4 receptor signaling in mice, Sci. Transl. Med. 14(655) (2022) eabj1895.
[70] J.S. Lee, R.X. Wang, M.S. Goldberg, G.P. Clifford, D.J. Kao, S.P. Colgan, Microbiota-Sourced Purines Support Wound Healing and Mucous Barrier Function, iScience 23(6) (2020) 101226.
[71] M.S. Lenucci, R. Tornese, G. Mita, M. Durante, Bioactive Compounds and Antioxidant Activities in Different Fractions of Mango Fruits (Mangifera indica L., Cultivar Tommy Atkins and Keitt), Antioxidants (Basel) 11(3) (2022).
[72] P. Wils, B. Caron, F. D'Amico, S. Danese, L. Peyrin-Biroulet, Abdominal Pain in Inflammatory Bowel Diseases: A Clinical Challenge, J Clin Med 11(15) (2022).
[73] A. Hurtado-Lorenzo, G. Honig, S.A. Weaver, P.B. Larkin, C. Heller, Chronic Abdominal Pain in IBD Research Initiative: Unraveling Biological Mechanisms and Patient Heterogeneity to Personalize Treatment and Improve Clinical Outcomes, Crohns Colitis 360 3(3) (2021) otab034.
[74] A. De Bernardi, C. Bezzio, M. Puricelli, D. Gilardi, S. Saibeni, Combining Advanced Targeted Therapy in Inflammatory Bowel Disease: Current Practice and Future Directions, Journal of Clinical Medicine 14(2) (2025) 590.
[75] M. Imran, M.S. Arshad, M.S. Butt, J.H. Kwon, M.U. Arshad, M.T. Sultan, Mangiferin: a natural miracle bioactive compound against lifestyle related disorders, Lipids Health Dis. 16(1) (2017) 84.
[76] A. Saviano, F. Raucci, G.M. Casillo, C. Indolfi, A. Pernice, C. Foreste, A.J. Iqbal, N. Mascolo, F. Maione, Present Status and Future Trends of Natural-Derived Compounds Targeting T Helper (Th) 17 and Microsomal Prostaglandin E Synthase-1 (mPGES-1) as Alternative Therapies for Autoimmune and Inflammatory-Based Diseases, Molecules 25(24) (2020).
[77] J.J. Jeong, S.E. Jang, S.R. Hyam, M.J. Han, D.H. Kim, Mangiferin ameliorates colitis by inhibiting IRAK1 phosphorylation in NF-κB and MAPK pathways, Eur J Pharmacol 740 (2014) 652-61.

[78] W. Dou, J. Zhang, G. Ren, L. Ding, A. Sun, C. Deng, X. Wu, X. Wei, S. Mani, Z. Wang, Mangiferin attenuates the symptoms of dextran sulfate sodium-induced colitis in mice via NF-κB and MAPK signaling inactivation, Int. Immunopharmacol. 23(1) (2014) 170-8.
[79] S. Danese, A. Gasbarrini, Chemokines in inflammatory bowel disease, J. Clin. Pathol. 58(10) (2005) 1025-7.
[80] K. Bielefeldt, B. Davis, D.G. Binion, Pain and inflammatory bowel disease, Inflamm. Bowel Dis. 15(5) (2009) 778-88.
[81] E.B. Okeke, J.E. Uzonna, The Pivotal Role of Regulatory T Cells in the Regulation of Innate Immune Cells, Front. Immunol. 10 (2019) 680.
[82] C. Zhang, Y. Li, Y. Yu, Z. Li, X. Xu, Z. Talifu, W. Liu, D. Yang, F. Gao, S. Wei, L. Zhang, H. Gong, R. Peng, L. Du, J. Li, Impact of inflammation and Treg cell regulation on neuropathic pain in spinal cord injury: mechanisms and therapeutic prospects, Front. Immunol. 15 (2024) 1334828.
[83] M. Zhao, J. Chu, S. Feng, C. Guo, B. Xue, K. He, L. Li, Immunological mechanisms of inflammatory diseases caused by gut microbiota dysbiosis: A review, Biomed. Pharmacother. 164 (2023) 114985.
[84] K. Gallagher, A. Catesson, J.L. Griffin, E. Holmes, H.R.T. Williams, Metabolomic Analysis in Inflammatory Bowel Disease: A Systematic Review, J. Crohns Colitis 15(5) (2021) 813-826.
[85] N. Kučuk, M. Primožič, P. Kotnik, Ž. Knez, M. Leitgeb, Mango Peels as an Industrial By-Product: A Sustainable Source of Compounds with Antioxidant, Enzymatic, and Antimicrobial Activity, Foods 13(4) (2024) 553.
[86] L. Keefer, J.G. Hashash, E. Szigethy, E.A. Mayer, AGA Clinical Practice Update on Pain Management in Inflammatory Bowel Disease: Commentary, Gastroenterology 166(6) (2024) 1182-1189.
[87] S.C. Lopes, A.V. da Silva, B.R. Arruda, T.C. Morais, J.B. Rios, M.T. Trevisan, V.S. Rao, F.A. Santos, Peripheral antinociceptive action of mangiferin in mouse models of experimental pain: role of endogenous opioids, K(ATP)-channels and adenosine, Pharmacol Biochem Behav 110 (2013) 19-26.
[88] B.B. Garrido-Suárez, G. Garrido, M. Castro-Labrada, N. Merino, O. Valdés, I. Rodeiro, I. Hernández, J. Godoy-Figueiredo, S.H. Ferreira, R. Delgado-Hernández, Anti-hypernociceptive effect of mangiferin in persistent and neuropathic pain models in rats, Pharmacol Biochem Behav 124 (2014) 311-9.

DECLARATION OF INTEREST

We wish to confirm that there are no known conflicts of interest associated with this publication and there has been no significant financial support for this work that could have influenced its outcome. We confirm that the manuscript has been read and approved by all named authors and that there are no other persons who satisfied the criteria for authorship but are not listed. We further confirm that the order of authors listed in the manuscript has been approved by all of us. We confirm that we have given due consideration to the protection of intellectual property associated with this work and that there are no impediments to publication, including the timing of publication, with respect to intellectual property. In so doing we confirm that we have followed the regulations of our institutions concerning intellectual property. We further confirm that any aspect of the work covered in this manuscript that has involved either experimental animal has been conducted with the ethical approval of all relevant bodies and that such approvals are acknowledged within the manuscript. We understand that the Corresponding Authors in the sole contract for the Editorial process (including Editorial Manager and direct communications with the office). They are responsible for communicating with the other authors about progress, submissions of revisions and final approval of proofs. We confirm that we have provided a correct email address which is accessible by the Corresponding Authors and which has been configured to accept email from anella.saviano@unina.it and francesco.maione@unina.it.

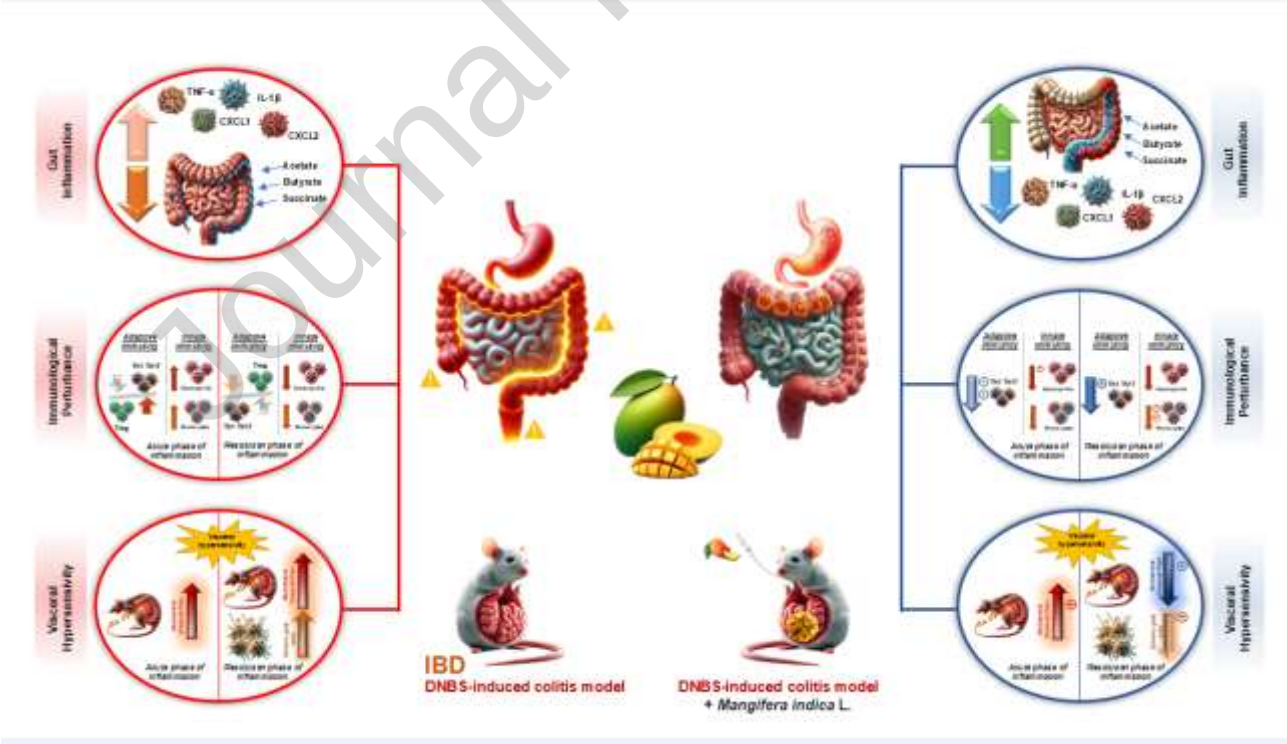

Highlights

- *MIE, rich in mangiferin, exhibited anti-inflammatory and analgesic effects in a colitis model.*
- *MIE reduced visceral hypersensitivity improving IBD-related quality of life.*
- *MIE reduced Th1/Th17 infiltration and cyto-chemokines, showing immunomodulatory effects.*
- *MIE restored SCFA levels (acetate, butyrate), suggesting gut microbiome modulation.*